INFORMATION TO USERS

This manuscript has been reproduced from the microfilm master. UMI films the text directly from the original or copy submitted. Thus, some thesis and dissertation copies are in typewriter face, while others may be from any type of computer printer.

The quality of this reproduction is dependent upon the quality of the copy submitted. Broken or indistinct print, colored or poor quality illustrations and photographs, print bleedthrough, substandard margins, and improper alignment can adversely affect reproduction.

In the unlikely event that the author did not send UMI a complete manuscript and there are missing pages, these will be noted. Also, if unauthorized copyright material had to be removed, a note will indicate the deletion.

Oversize materials (e.g., maps, drawings, charts) are reproduced by sectioning the original, beginning at the upper left-hand corner and continuing from left to right in equal sections with small overlaps.

Photographs included in the original manuscript have been reproduced xerographically in this copy. Higher quality 6" x 9" black and white photographic prints are available for any photographs or illustrations appearing in this copy for an additional charge. Contact UMI directly to order.

ProQuest Information and Learning
300 North Zeeb Road, Ann Arbor, MI 48106-1346 USA
800-521-0600

Laminar Burning Velocity Measurements of Stabilized Aluminum Dust Flames

Massimiliano Kolbe

A Thesis

in

The Department

of

Mechanical Engineering

Presented in Partial Fulfillment of the Requirements
for the Degree of Master of Applied Science at
Concordia University
Montreal, Quebec, Canada

July 2001

ABSTRACT

Laminar Burning Velocity Measurements of Stabilized Aluminum Dust Flames

Massimiliano Kolbe

The laminar burning velocity of a stabilized dust flame is experimentally investigated in the present work. The dust used was aluminum powder with an average particle diameter of approximately 5 microns. Dust flames, in comparison to gas flames, are thicker and brighter, may be influenced by radiation heat transfer, respond differently to heat losses, and are influenced by the particular flow configuration due to the particle's inertia. With the apparent sensitivity to a specific experimental apparatus, the introduction of a fundamental flame speed or burning velocity may be problematic for dust combustion. The present work investigates to what degree burning velocities obtained from Bunsen dust flames depend on experimental conditions (i.e. flow rate and nozzle diameter). The current experimental apparatus permits the stabilization of aluminum-air dust flames using conical nozzles and the accurate measurement of dust concentration. Experimental results show that burning velocities in aluminum-air suspensions increase considerably with the increase in flow rate but decrease with the increase in nozzle diameter. Theoretical estimations show that radiation heat transfer effects are small and cannot explain the observed experimental trends. The present analysis of dust flames shows that the observed effects are primarily the result of flame curvature and of larger flame thickness as compared to gas flames.

Acknowledgements

The author wishes to express his gratitude to his co-supervisor Dr. John H.S. Lee who initiated and supported this research providing the much-needed courage to always persevere in the research effort no matter what the circumstance. Much gratitude is also extended to Dr. Samuel Goroshin for providing all the essential technical and theoretical support throughout the experimental investigation.

Finally, the author wishes to extend his gratitude to his co-supervisor Dr. Rafik Neemeh for providing continued guidance and helpful comments specifically in the final stage of this investigation.

I wish to thank Charlene Wald for all her help and patience, Machinists and Mechanical technicians (Tony, Garry, John and Ray) for bringing to reality what I could only draw on paper. I also wish to thank all of my close friends at the Shock Wave Physics Group at McGill University for providing me with an audience for my comedy and home for the past few years!

Finally, I wish to express all my gratitude, love and admiration to my mother and father, zia Wanda, Antonio, my brother Paul and my sisters Laura and Marina for being caring, supportive and always providing me with a positive outlook when I needed it the most.

The author gratefully acknowledges the financial support received for this research from the Canadian Space Agency under the Microgravity Science Program.

Table of Contents

List of Figures

List of Tables

List of Special Symbols

d_{32}	Mean particle Sauter diameter
d	Focal lens aperture diameter for light extinctiometer
I_0	Incident light intensity
I	Transmitted light intensity
k	light attenuation curve constant
x	Dust flow path thickness
N	Number of particles
s_0	Sauter cross section
B	Dust concentration
r	Particle radius
ρ	Particle density
Φ	Equivalence ratio
S_u	Burning velocity
S_u^0	Unperturbed burning velocity
$\mathcal{L}$	Characteristic length
L_{th}	Thermal length
μ	Ratio of characteristic length to thermal length
δ	Total dust flame width
δ_c	Dust flame combustion zone length
δ_p	Dust flame pre-heat zone length
T_g	Gas temperature

T_s	Particle temperature
$\bar{A}$	Average value of flame thickness to flame radius ratio
H_0	Flame height
R_{flame}	Radius of curvature of flame
R_0	Radius of flame base
$r(h)$	Polynomial equation approximating flame profile

Chapter 1
Introduction

The mechanisms that govern the physical and chemical processes that occur within dust flames have been the subject of much debate. Knowledge of fundamental combustion parameters, such as the laminar burning velocity, are essential in understanding and in describing the physical and chemical processes that manifest themselves in dust flames. Many methods have been used to study laminar burning velocities of dust flames; however, the results have seldom been in agreement. Homogeneous gas flame burning velocities have long been studied using the well-known Bunsen burner and much is now understood of the mechanisms involved in gas flame combustion. Heterogeneous flames, or dust flames, have not been studied to the same extent, and a fundamental tool such as the Bunsen burner has not been validated for dust flames. There is therefore a need for further understanding of dust flames as well as a need for reliable data gathering by some proven apparatus. This thesis presents a detailed experimental investigation of the laminar burning velocity of Aluminum dust flames stabilized on a Bunsen-type burner.

In the following chapter, an introduction to the field of dust combustion will be presented by first discussing the applications of dust combustion science in industry and brief review of dust combustion experiments carried out by past investigators followed by a discussion of the thesis objectives

1.1 Practical Applications

The motivation behind dust combustion research originates from the first careful observations of firedamp explosions in coal mines, which were a very serious threat to the mining industry. Davy's safety lamp in the early 19^{th} century was a response to coal mine explosions, but it failed to recognize an important secondary hazard commonly encountered in coal mines. It was only several years later, that suspensions of coal dust particles were first recognized by Faraday as a determining factor in mine explosions, and it was carefully mentioned in his 1844 report on the disastrous mine explosion at the Haswell colliery. Since then, combustion study of suspended particles (more commonly known as dust combustion) has had many important implications not only in the field of safety standards but in power generation, propulsion technology and, recently, in the technology of nano-scale particle synthesis.

The prevention of gas explosions or fires in industry has been a very important research topic for safety standards. In the case of coal mines, the main safety concern is the prevention of coal dust suspensions that could potentially form extremely violent secondary explosive mixtures when preceded by methane-air explosions[1]. In many well-documented situations, methane gas leaks/formations would occur in coal mines and form potentially hazardous conditions. When these gaseous mixtures would accidentally ignite, they would lead to extremely violent explosions. Many sources of ignition or hot surfaces such as constantly operating heavy machinery, high power pumps and heavy power tools (i.e. pneumatic hammers and drills) exist in an average mine. Local methane explosions or fires can create pressure waves strong enough to entrain surrounding coal dust from

surfaces and floors into dust cloud suspensions. Given the right conditions, dust clouds may ignite, and the flames can propagate through the dust suspension and develop into violent explosions that are several times more powerful than gas explosions, causing extensive damage, injury and even death to nearby miners. In the United Kingdom during the years 1962 to 1980, there were 485 explosions and 715 fires reported in underground mines caused by flammable dust suspensions, resulting in 26 fatalities and 639 injuries[2].

Agriculture is another area where dust explosion safety standards have been implemented due to many situations where particulate suspensions have caused disastrous explosions. Centralized grain processing stations are used to store vast quantities of grain, wheat and flour. The common method of transportation within these stations is via pneumo-transport; typically, the use of pumps to siphon the product form silo to silo, or to train loading cars nearby, is employed in such buildings. These transporting processes inevitably form large and potentially explosive clouds of suspended dust particles that require only a minimal ignition source which can be easily provided by the heat given off by constantly running machinery. In the United States, the Department of Agriculture reported 129 grain dust explosions between 1987 and 1997; more recently, in 1998, a grain dust explosion in a grain elevator near Wichita, Kansas, caused 7 deaths and 10 injuries[3]. The following pictures (Fig.1 and Fig.2) illustrate situations where wheat and grain explosions have caused extensive structural damage to silos and storage facilities.

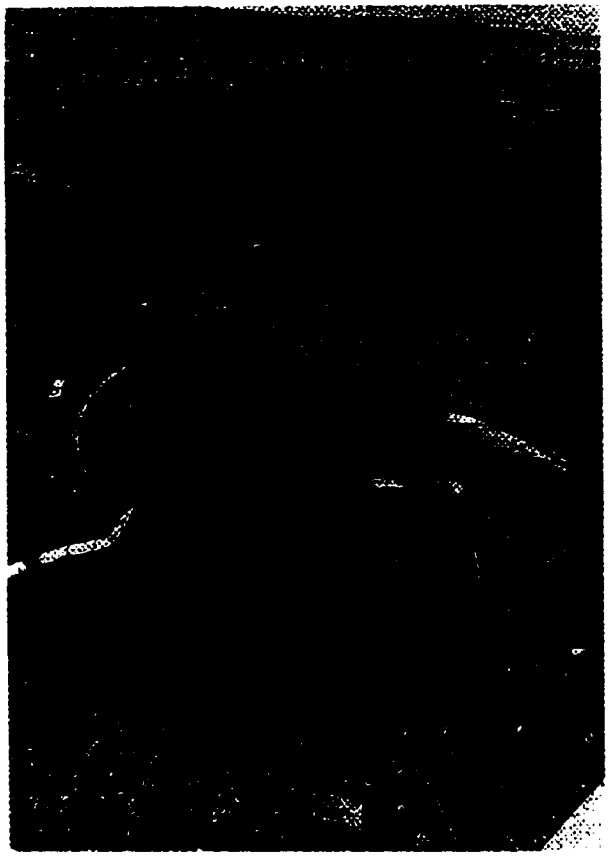

Figure 1: Silo roof damage due to a wheat grain explosion, Norway 1970. The extent of the damage caused can be seen by noting the worker situated at the top part of the damaged concrete roof.

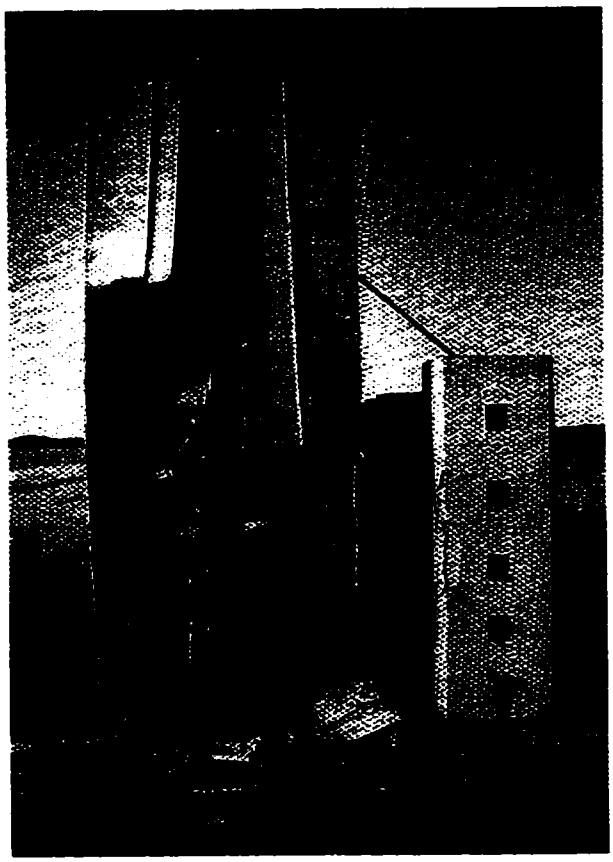

Figure 2: Storage silo damaged by a grain dust explosion, Norway 1976. Dust explosions generate overpressures that are several times greater than gas explosions, as can be seen by the damage created on the building.

Although dust suspensions have been the cause of many devastating accidents, the energetics of dust combustion have had important implications and even desirable effects in the field of power generation. The majority of the world's energy supply stems from the burning of fossil fuels. In the United States, coal combustion is the 3rd highest energy consumption source, measuring 22.17 quadrillion Btu's in the year 2000 alone[4]. Dust combustion research has made important advances and improvements in coal combustion efficiency. Pyrolysis, or devolatilization rate, is a process by which dust particles break down from their solid state forming a better gas-phased mixture for increased combustion rates. In organic based particles, this process is mainly influenced by the particle size. Devolatilization in organic materials precedes the combustion process, thus the role of particle size in dust combustion is of primary importance. By decreasing particle diameter, the specific surface area can be increased significantly and thus increase the rate at which individual particles devolatilize. Because most solid fossil fuels are presently burnt in pulverized form, it has been found that the high specific surface area of dust particles makes it possible for dust combustion to attain heat release rates comparable to gaseous reactions[5].

The energetics of dust combustion are not only limited to power generation but have also been extended to other applications such as solid fuels in the propulsion industry. The field of dust combustion has been a centerpiece in the area of solid-fueled rocket propulsion. As mentioned earlier, particle size has proven to be a key factor in the combustion process of solid particulate fuels. For a particulate fuel such as coal, the limiting size of the particle where the combustion rate can no longer be increased is

approximately 50 microns[6]. In other words, any further reduction in particle size will not increase the devolatilization rate (which will, in turn, increase the combustion rate). However, for metals this is not the case, and the limiting particle size is several times smaller than that of organic based powders. In a combustion process, metal particulates do not devolatilize but melt, evaporate and then combust as individual particles. This makes metallized powders much more sensitive to combustion and, therefore, extremely energetic. Many light metals such as boron, beryllium, aluminum and magnesium, possess heat production capacities that are only exceeded by hydrogen as seen in Table 1 [7].

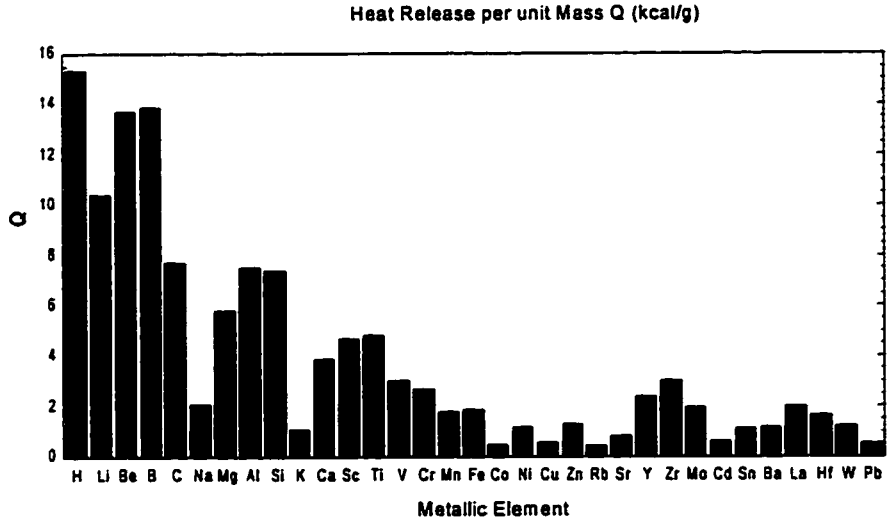

Table 1: Heat release of typical metallic elements.

Much research carried out during the 1960's in the propellants industry has made use of many discoveries and advances in dust combustion research. Metallic based particle combustion became a research topic that commanded a great deal of attention when it was found that very high theoretical specific impulses were obtained by combining various

solid propellants with metal additives[8]. Many other advances were made in rocket propulsion such as jelled propellants with metal additives and feasibility studies of ramjet engines using various pulverized energetic metals as a primary fuel source [9].

Dust combustion research has also found much use in nano-scale particle production, where such materials as $AlNO_3$ are produced from high-pressure combustion of aluminum powder. Aluminum Nitrates are widely used in the micro-chip industry for their remarkably high heat conductivity and are therefore used for cooling purposes. Dust combustion processes have the potential to yield very pure nano-sized, spherical oxide particles (less than 0.1 microns). Further reduction of particle sizes in ceramic aggregates has solved many problems encountered in ceramic materials such as brittleness. Metal powders are widely used in present day industry like powder metallurgy and paint production, for example. The production rate of industrial powders by developed countries has now reached a thousand tons per year. The safety expenses related to explosion prevention associated with the handling of these materials can account for a considerable part of production costs. In other words, these expenses, in terms of financial and human damage caused by accidental situations, can be enormous. For example, due to the extreme flammability of certain powders (when mixed in air) many metallic powders are produced in oxygen free or oxygen reduced atmospheres. This type of procedure requires strictly controlled environments that can be very costly to maintain but obviously less costly to the industry than to sustain accidental explosion damage.

Another application of metallic powder technology, more specifically aluminum powder, is in many of the paints used in present day industry. Special doping compounds that are mixed with today's paints give desirable characteristics to surfaces that are constantly exposed to climate changes or harsh environments, making the painted surface more durable. Unfortunately, many of the hazards described above are by no means excluded in this application of metallic powders. Often these paints have shown to be extremely flammable in the past both from their applications to their production. An interesting example is the one of airship design in the earlier part of the 1900's. The well-known Zeppelin airship manufacturer, which constructed the Hindenberg, was victim to such a paint hazard[10]. Recent investigations have shown that the explosion or fire that brought down the dirigible was due to a static electricity driven spark that ignited the textile material that was used to cover the dirigible. The textile was covered with a paint that contained high levels of aluminum and iron oxide powders (now found in many rocket motors) that formed a doping compound. This was done to enhance the textile's strength, color and durability while subjected to extreme climate changes. This mixture of powders is, however, highly reactive when subjected to an ignition source. After the disaster the Zeppelin company later altered the doping agent in the paints to a none flammable mixture.

Whether it be in the prevention of dust flames and explosions, the use of more efficient and environmentally safe coal combustion, the improvement of propellants or production of advanced materials, dust combustion research has helped gain an understanding on many of the mentioned issues. Given the important roles that dusts and

powders represent in present day industry, fundamental understanding of the basic mechanisms governing heterogeneous combustion is not only necessary but essential to the general field of combustion. Unfortunately, despite its importance, heterogeneous combustion has received only a small fraction of the attention that homogenous or gas combustion has received in combustion research. Much of this lack in knowledge is attributed to many of the complexities involved in heterogeneous or multi-phase combustion and has thus made dust combustion more of an empirical study with very little theoretical understanding of the basic combustion parameters. Dust combustion research has many experimental difficulties that are not typically found in gas combustion, such as uniform dispersion of solid fuel particles or (when required) controllable laminar flows of dust-air mixtures. The high diversity of solid fuels, in comparison to gaseous fuels, makes dust combustion research a more complex and vast field of study. In many cases, different hydrocarbon fuels have similar chemical and physical properties. Solid fuels, on the other hand, can be organized into many categories. Their physical nature (metallic or non-metallic), chemical properties, volatility and other characteristics that contribute to many diversified fuels, yield very different combustion characteristics per given fuel. In addition to these problems, the two-phase fluid mechanics and thermodynamics involved are challenging topics even without the added complexity of a combustion process.

1.2 Review of Dust Combustion Research

The initial investigations in dust combustion originally begun by Nusselt[11] were first setup to understand the dust combustion processes in coal suspensions. It was realized that many regimes influenced single particle combustion and that one regime was the process of oxygen diffusion over the particle's surface. This seemed to be a dominant factor in the combustion process. Nusselt also suggested that radiation heat transfer effects of burning particles might play some role on the propagation of a flame in a large enough dust cloud. Nusselt later predicted the possibility of a stabilized dust flame (similar to a Bunsen burner gas flame) and the formation of an inner cone in the stable flames. Since those pioneering days, a lot of research in the coal combustion field was carried out; much data was obtained on explosion pressures and flame propagation in coal dust clouds. However, very little reliable data was obtained on such fundamental combustion parameters as the laminar burning velocity.

Due to such a lack of fundamental research in dust combustion, there has been no agreement as to what is the governing mechanism of combustion in dust suspensions. Through research, processes that are involved in gas flame propagation such as heat conduction and molecular diffusion have been identified. In dust combustion, the significance of molecular diffusion and heat conduction or what role, if any, radiation plays in dust flame propagation have failed to be proven. It is well known that gas flames propagate mainly due to thermal and molecular diffusion and that radiation has little or no influence in flame propagation. However, no such definite claim has yet been made in dust combustion, and the absence of a detailed study in dust flame structure becomes evident.

In contrast to homogeneous gas combustion, there is difficulty controlling "clean" experiments in dust combustion. Many problems such as sedimentation, particle agglomeration or uniform dispersion of dust are not trivial issues to solve. The main difficulty is producing a uniform dispersion of a dust in a mixture for a given controlled environment.

The majority of efforts in dust combustion research were using the closed vessel apparatus or constant volume dust explosions (sometimes known as a Hartmann bomb). In this setup, a vessel is sealed and pressure probes are distributed inside the vessel (Fig. 3). A dust dispersion system is triggered (usually a syringe injects a dust mixture with a burst of air) and a cloud of dust is left to fill the vessel. Often, a certain amount of time is given to allow the dust to become quiescent, After which, an igniter (electrode spark or pyrotechnic match) is made to ignite the dust cloud. Such experiments were made primarily to investigate explosion pressures for industrial safety parameters. Closed vessel experiments are very common in dust combustion and a variety of dusts, from organic to non-organic, have been tested in them. Many parameters such as dust concentration and particle size have been tested. However, the problems of particle settling and agglomeration have made measurements of laminar burning velocity extremely difficult. Ignition could sometimes trigger a deflagration in an otherwise non-ignitable mixture due to a localized high concentration pocket of dust. In other words, the laminar burning velocity is a very important and fundamental parameter that closed vessel experiments failed to yield accurate data on.

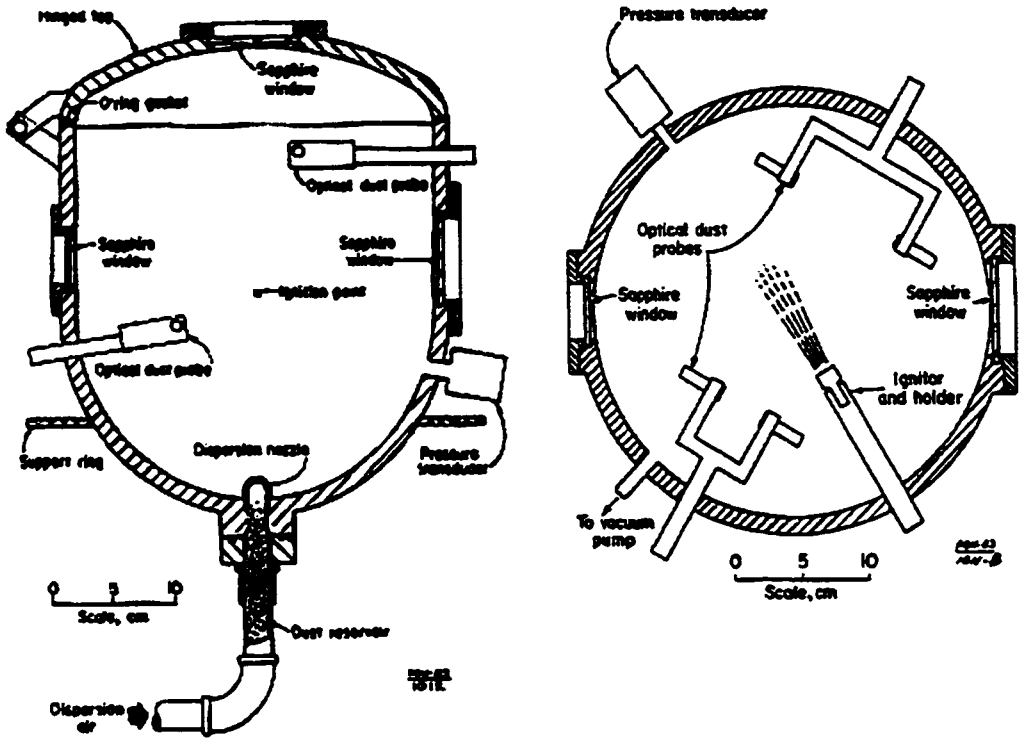

Figure 3: A 20-liter explosibility test chamber used by the Bureau of Mines in Pittsburgh, PA, USA. The schematic on the left shows the chamber in vertical cross section and the right view shows a horizontal cross section.

Another apparatus that was employed in dust combustion research was the glass tube to carry out flame propagation experiments. Many experiments measuring flame speeds and quenching distances in dust mixtures have been done in such an apparatus. The flame tube gave an opportunity to examine the quiescence of the dust mixture and to ensure that the dispersion is uniform while, at the same time, enabling flame speed or quenching distance experiments to be carried out. The flame tubes consisted of glass cylinders in which a dust was dispersed with air or some other oxidizer. The mixture was

flowed through the tube and when the desired concentration was reached, the flow was stopped and then ignited. The flame would then propagate either upwards or downwards depending on the position of the ignition source. Visual observations were made by measuring arrival time of the flame at various markings on the tube. Although more accurate and "cleaner" experiments were possible, other problems were being recognized with flame propagation in dust clouds. The problem of non-turbulent and uniform dispersions was not completely solved. In addition, dust flames turned out to be much brighter and thicker than gas flames. Dust sedimentation was observed for large particle sizes and the fluid mechanics involved in multi phase flows and their effects on boundary conditions became a challenging problem to solve. Other problems inherent with the flame tube apparatus involved flame stretching at the tube walls, acoustic coupling effects (altering the shape of the flame) and buoyancy effects which appeared to be enhanced due to the slower velocities (compared to gas flames) that dust flames seemed to exhibit. Burning velocities (in micro-gravity experiments) as high as 30 cm/s to 40 cm/s in lean aluminum air mixtures have been reported in particle size dusts of 10 microns by Ballal et al. showing a square root dependence on increasing concentration[12].

Some problems were solved. Brightness was reduced by the use of optical filters on photographic equipment. The particle sedimentation could be solved by performing experiments in micro-gravity environments such as, parabolic flights in aircraft, sounding rockets or drop tower experiments. However, all the experiments still yielded varying results on burning velocities of the same type of dusts and the experiments seemed to be apparatus dependent in many cases. Past experiments by Goroshin et al. in dust flame

propagations have shown that within the fuel rich regime of aluminum air mixtures (above 350 g/m^3) the flame speeds show a weak dependence on dust concentration[13]. This observation was reproducible for many other metallic based fuels and seemed to be a characteristic feature of dust flames. Unfortunately, data from flame propagation experiments could not accurately describe the dust flame burning velocity, mainly due to the unclear definition of the dust flame profile and the mechanisms governing the various stages of combustion in a dust flame.

Historically, a common tool used in gas combustion experiments to measure laminar burning velocities has been the Bunsen burner. Burning velocity studies in homogenous mixtures have been extensively investigated in Bunsen-type burners. A great deal of data has been obtained from these burners. Although many effects such as curvature and rim heat losses have slightly reduced the accuracy of burning velocity measurements, stabilized flame burners are generally viewed as an accurate tool in measuring burning velocities in homogeneous combustion. Since this tool is of great importance in gas combustion, its implementation in dust combustion is a logical step. The main difficulty was still in a uniform dust dispersion mechanism, although particle settling was one less problem since the dust flow is maintained continuously in a burner.

One of the first successful research efforts to produce a stable dust flame was pioneered by Cassel in the 1960's [14]. He was able to obtain burning velocities of metallic fuels such as magnesium and aluminum on which very little combustion knowledge was available. Cassel was able to record data and stabilize aluminum-air

flames on a conical nozzle and a flat flame burner as well. Investigations were carried out in the fuel-lean regime of aluminum-air suspensions, between 100 g/m^3 to 250 g/m^3 (the stoichiometric fuel ratio being 310 g/m^3). For particle diameters of less than 10 microns, the burning velocities range from 18 cm/s to 42 cm/s, increasing with dust concentration. For particle diameters less than 30 microns the burning velocity increased from 12 cm/s to 25 cm/s with increasing dust concentration. Cassel was also able to experiment with varying nozzle diameters and noticed that there was an increase in burning velocity with decreasing nozzle diameter[15]. Another trend that was observed was that of the dependence of the burning velocity on the square root of dust concentration, from lean to rich. The same trend was observed for the dependence of burning velocity on oxygen concentration when the O_2 increased from 21 % to 100 % in an O_2-N_2 mixture. Cassel's results led him to conclude that the dust flame's burning velocity was a function of burner size. Later, experiments by Goroshin et al. that made use of a dust burner to stabilize rich aluminum dust flames revealed a weak dependence of burning velocity on concentration (in the rich mixture regime) [16].

1.3 Thesis Objectives

Since Cassel's work, very few have been successful in reproducing a dust flame burner using metal fuels, and most work in dust combustion continued mainly with flame propagation experiments. In addition, few attempts have been successful in providing a clear model of how dust flames propagate. This is mainly due to the lack of reproducible fundamental combustion data and the many difficulties involved in constructing a reliable dust burner.

The concept of using burning velocity as a means of understanding the thermo-chemical principles in dust combustion is to be questioned. It was found necessary to verify the reliability of the dust flame Bunsen burner as a tool for measuring burning velocity and to solve the problem of apparatus dependence in dust combustion data. The laminar flame speed, more commonly known as burning velocity, is a very important and fundamental combustion parameter that describes the basic heat and mass transfer processes in a reaction zone. If a reliable dust flame model is to be constructed, accurate knowledge and reproducible data of dust flame burning velocities must be obtained. The last successful attempts on aluminum dust flame Bunsen burners were limited to fuel-rich dust regimes and made use of cooling rings to stabilize dust flames. Improvements such as in-situ dust concentration measurements as well as accurate dust flow monitoring have also been implemented in the present research efforts.

The objectives of the following work are to verify the validity of the dust flame Bunsen burner as an accurate tool for measuring the burning velocity of stabilized aluminum dust flames and to investigate the concept of laminar burning velocity in aluminum dust flames.

Chapter 2
Experimental Setup

The primary reason for the lack of reliable data in the field of dust combustion has been due to the difficulties involved in dust dispersion, efficient mixing of dust particles in the oxidizing gas and finally laminarization of a turbulent dust flow mixture. The following chapter will begin by giving a detailed description of the apparatus used in this investigation and the methods used to overcome the above mentioned difficulties.

The dust concentration measurement setup is a key element in dust combustion experiments, and a variety methods exist to measure dust concentrations. The second section will describe the light extinctiometer used to measure dust concentration, and the third section will give a brief description of the aluminum dust used.

Since aluminum dust flames were found to be very bright, it was necessary to experiment with a variety of photographic techniques and equipment. The fourth section will describe the procedure used in obtaining the stabilized flame pictures, and the final section will describe the complete procedure followed in obtaining a stable dust flame during a typical experimental burn.

2.1 The Dust Burner

A general schematic of the experimental apparatus or "dust burner" set-up is displayed in Fig.4. Contrary to the gas flame Bunsen burner, the dust flame Bunsen burner involves a great deal of attention to technical detail and makes use of many devices to successfully stabilize a dust flame. In general, the dust burner is not capable of continuous fuel injection the way a gas burner is. In other words, it makes use of a syringe-like or piston-cylinder assembly to inject discrete amounts of dust per experimental trial. The typical experimental time span is approximately 5-6 minutes, from which a stable flame can be achieved for up to 4 minutes. The main difficulty in dust combustion lies in the uniform dispersion of a dust sample in a gas. In order to evenly disperse a dust mixture, the dust pile surface must be subjected to intense turbulence in order to dislodge the particles from each other to avoid agglomeration.

The cylindrical steel housing, in which the dust is contained, guides the piston, which pushes the dust sample upwards. The piston is appropriately equipped with sealant rings to prevent dust from seeping along the cylinder walls and possibly jamming the piston into an unwanted position. The piston rod speed is controlled by means of an electro-mechanical actuator. This enables the speed of dust injection or dust feeding rate to be electrically controlled by means of a variable potentiometer. The dust is forced upwards through a slight conical contraction. Another cylindrical housing in which regular dry air (supplied by a gas bottle) is fed, surrounds this contraction. As both dust and air travel separately upward, they are finally mixed when the air is forced into a circumferential channel (very small in height and set at an approximate upward angle of 30 degrees) that

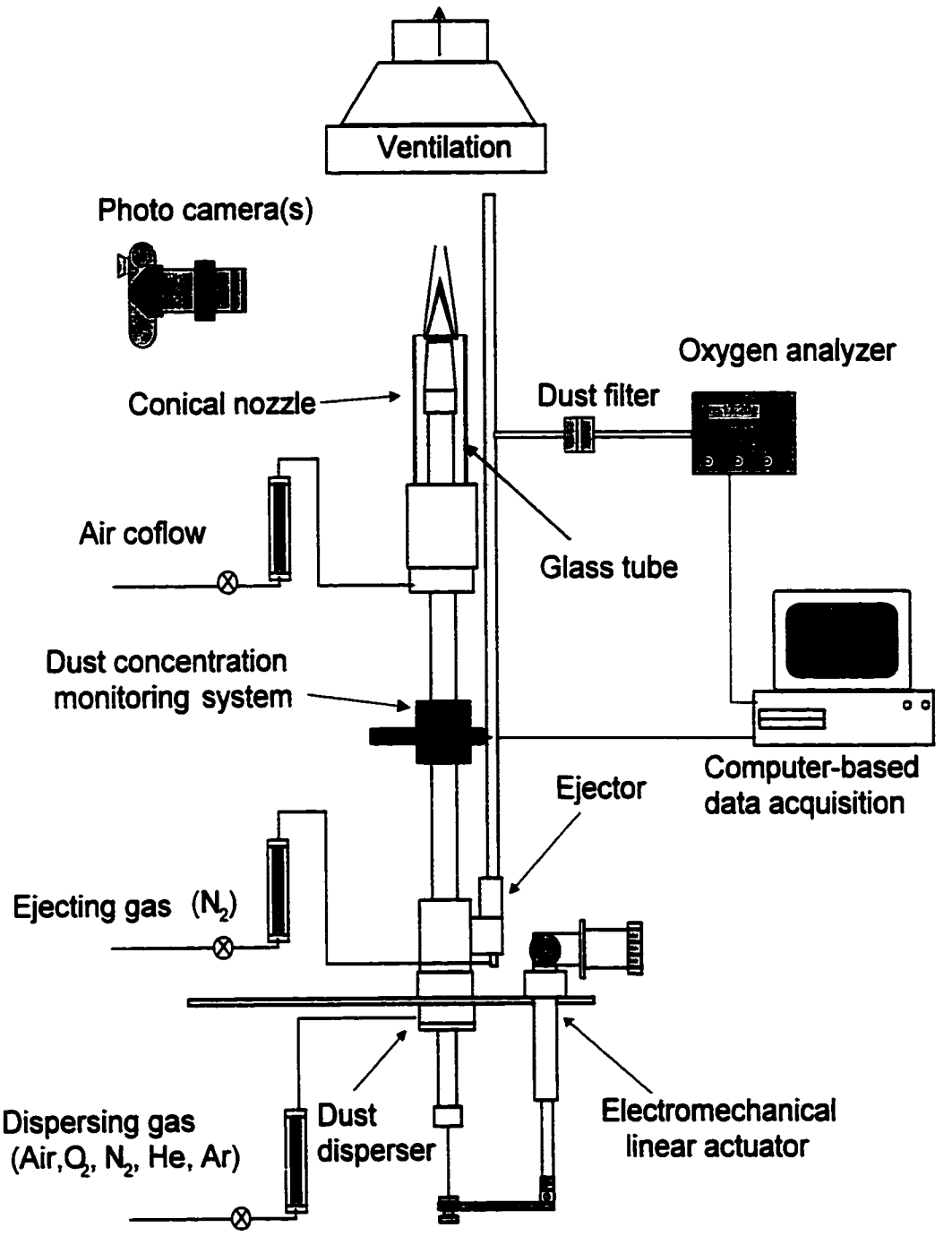

Figure 4: General schematic of the Dust Burner showing all the main peripheral equipment (ie. Photographic cameras, PC data acquisition, Oxygen Analyzer)

encounters the upward moving dust pile and entrains it upward (Fig. 5). By forcing the air jet through the very small slot (20 microns to 40 microns in height), a very high rate of shear is created and this is sufficient to provide the necessary turbulence to dislodge the dust particles. Now that a uniformly mixed dust-air mixture is present, it is very turbulent and must be laminarized without settling the mixture. This is achieved by expanding the dust flow through a diffuser and slowing the dust flow while allowing it to still travel upwards.

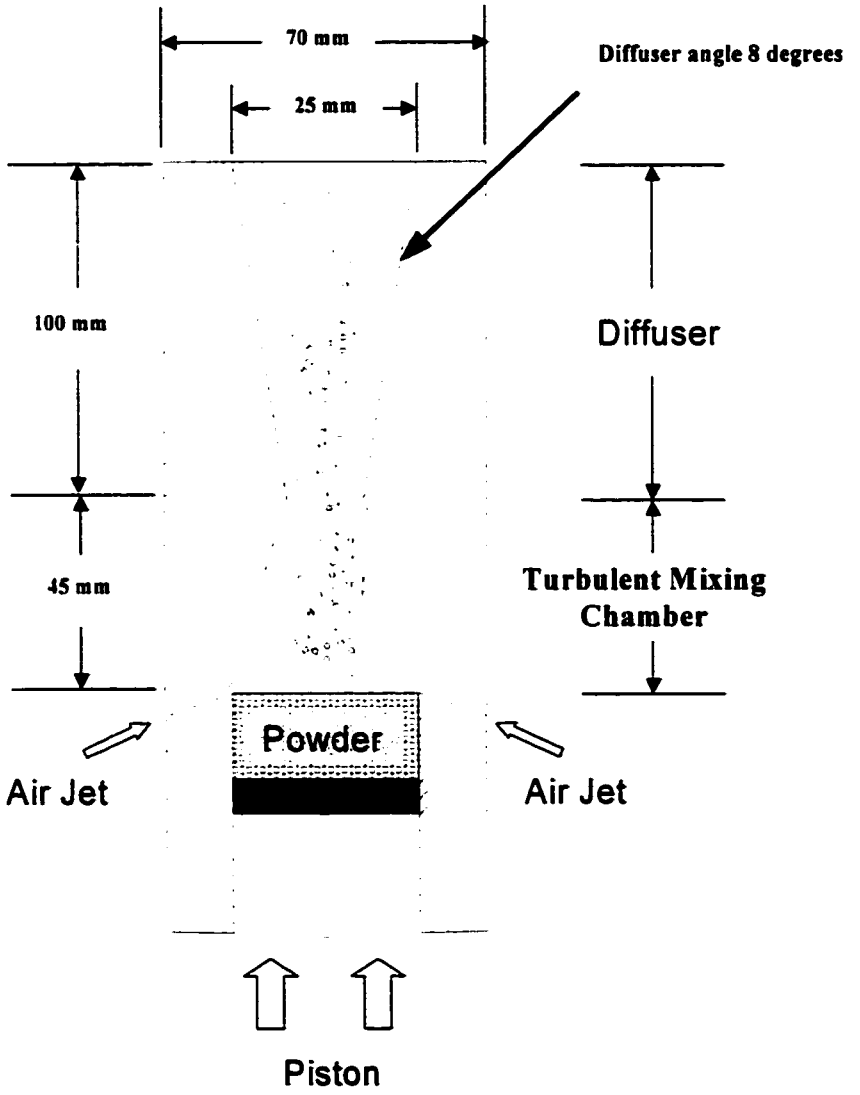

Figure 5: Cut-away close-up of the dust dispersing mechanism. Note, drawing not to scale.

At this point, a laminar dust-air mixture is created and is made to flow up into a cylindrical channel that has an elbow-like brass fitting in the center of the flow, much like a pitot tube in a flow field (Fig. 6). This brass elbow fitting is called the ejector and has the ability to decrease or increase the dust flow without affecting the dust-air dispersion or concentration. The ejector connects the main burner tube to a smaller bypass side tube. This calibrated ejection system ejects a required part of the dust flow from the incoming main stream to the side bypass tube, thereby incrementally regulating the dust flow. The amount of flow ejected is controlled by varying the inlet pressure inside of the bypass tube by increasing or decreasing the gas flow rate through the tube itself. The ejector gas consists of standard grade extra dry nitrogen supplied by a nearby gas bottle.

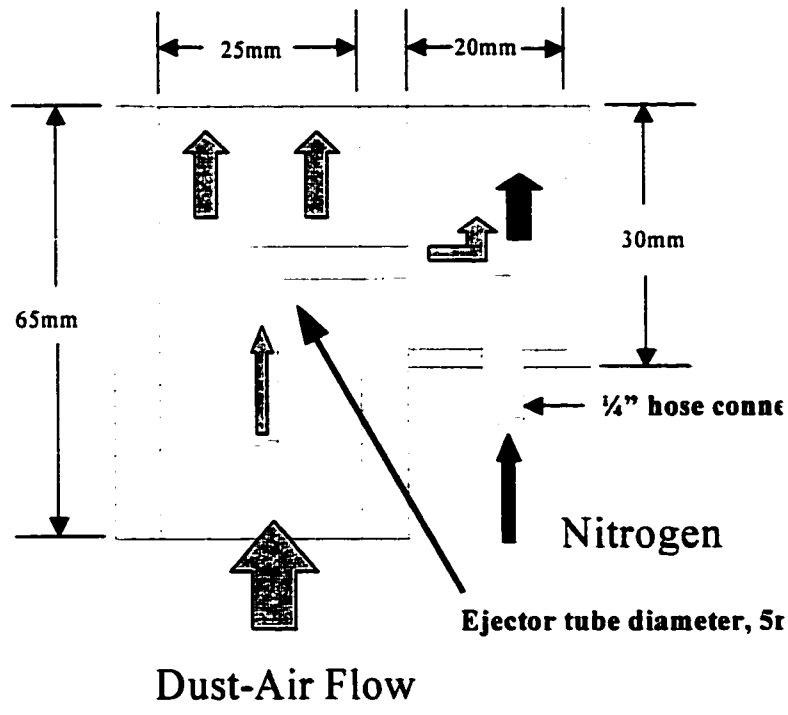

Figure 6: Cutaway view of the ejector showing the main burner tube and the smaller bypass tube. Note, drawing not to scale.

Since pure nitrogen is used as the ejecting gas, the dust air flow removed from the main stream by the ejector can be easily calculated by measuring the concentration of oxygen in the bypass tube. Oxygen concentration in the ejector flow is continuously monitored by an in-line electrolytic oxygen analyzer and is recorded by a computer data acquisition system.

Following the location of the ejector are two sections of stainless steel tubing of 25 mm diameter cross section that make up the main burner tube. A brass connector, which houses the optical dust concentration measuring device and will be discussed later in detail, joins these two steel tube sections. The combined steel tubes form a 70 cm long channel with smooth inner walls maintaining laminarization of the dust-air flow after mixing occurs of the air and dust at the dust feeder stage near the base of the apparatus.

Resting on the brass connector is a glass tube of 10 cm in diameter that encompasses the second upper steel tube. Regular dry air (again supplied from a gas bottle) is made to flow in this glass tube at relatively low flow rates to provide an enveloping blanket or protective co-flow for the exiting dust air flow (Fig. 7). This co-flow exists so that the dust-air mixture remains in a laminar, column-like form once it exits from the conical brass nozzle and recirculation eddies forming at the nozzle exit can be prevented. The actual flow through the nozzle is measured via rotameters mounted on the control panel. The control panel consists of a disperser, a co-flow and an ejector rotameter; all of which are regularly calibrated.

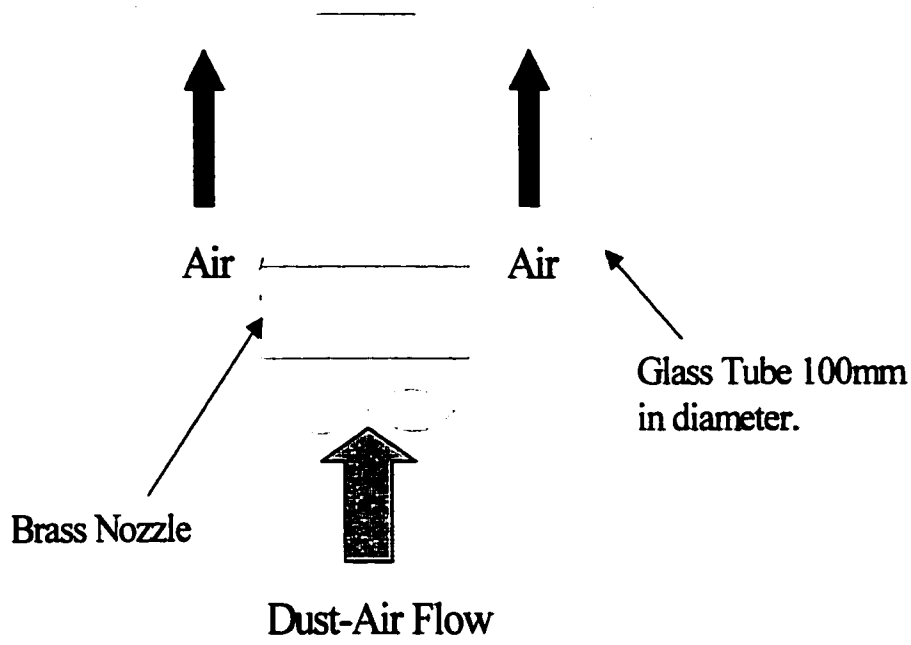

Figure 7: Cutaway view of the co-flow setup.

The dust flow finally exits the tube though a conical brass nozzle. Other nozzles of varying contraction angles can be placed at the tube exit. The nozzle diameters used for this investigation were of 14 mm, 18 mm and 21 mm in diameter at the exit. All nozzles were of the same height, material and base diameter. Previous experiments by Goroshin et al. made use of a water-cooled detached ring (several millimeters above the nozzle) to stabilize dust flames [16]. The flame directly stabilized on the nozzle, instead of a detached ring, eliminates the uncertainty in flow rate that might occur from gas entrainment into the flame from the surrounding atmosphere beneath the cooling ring.

The dust flow ignition mechanism consisted of a Methylacetylene Propadiene (MHP) hand held torch (commonly used for brazing or soldering) mounted near the nozzle exit and an electrical spark igniter was used to remotely light the torch. Once a stable, self-sustained flame was achieved, a solenoid valve was used to shut off the torch gas supply. Originally, a regular propane soldering torch was used to ignite the dust flow. It was found that the regular propane torch did not yield a high enough temperature to easily ignite a dust flame; whereas the MHP torch yielded a flame temperature of about 2200 K which was a few hundred degrees higher than the regular torch and provided a quicker ignition of the dust flow.

2.2 Optical Dust Measuring Device

With the flame anchored at the nozzle exit, the dust concentration is monitored directly within the dust supply tube by the laser light extinctiometer (Fig. 8). In this design, the light emitted by the 3 mW laser diode is introduced into the dust tube through airflow protected windows and then the dust flow, it then passes through a narrow channel and is focused by a long focal lens on a small aperture (d = 0.25 mm). The aperture plays the role of a spatial filter that cuts scattered laser light thus making deviation from the Bouguer's light attenuation law negligible even for optically thick dust clouds. A narrow bandwidth interference filter permits only the laser light to pass, protecting the photo detector from the scattered light emitted by the flame. The signal from the photo detector is amplified and recorded by a computer data acquisition system. The laser light extinctiometer was calibrated by the complete aspiration of dust from the nozzle flow through a set of surgical mask filters with a vacuum pump for a known time. Dust mass concentration in the flow is then determined by dividing total mass of the aspired dust by the volume of the gas passing through the nozzle during the same time. The calibration curve for the light extinctiometer is shown in Fig. 9. Mean particle Sauter diameter (d_{32}) in a suspension can be calculated from the data shown in Fig. 9 by using Beer's light attenuation law[17]. The calculations indicate an average particle diameter of 5.2 μm. Due to Mie's theory on diffraction, the light attenuation cross section for particles of this size is twice the size of the particle cross section [17]. This value practically coincides with the average Sauter diameter derived from the particle size distribution shown in Fig. 10 (d_{32} = 5.8 μm), which confirms that the particle agglomeration in the dust flow is negligible and that a uniform dust mixture has been achieved.

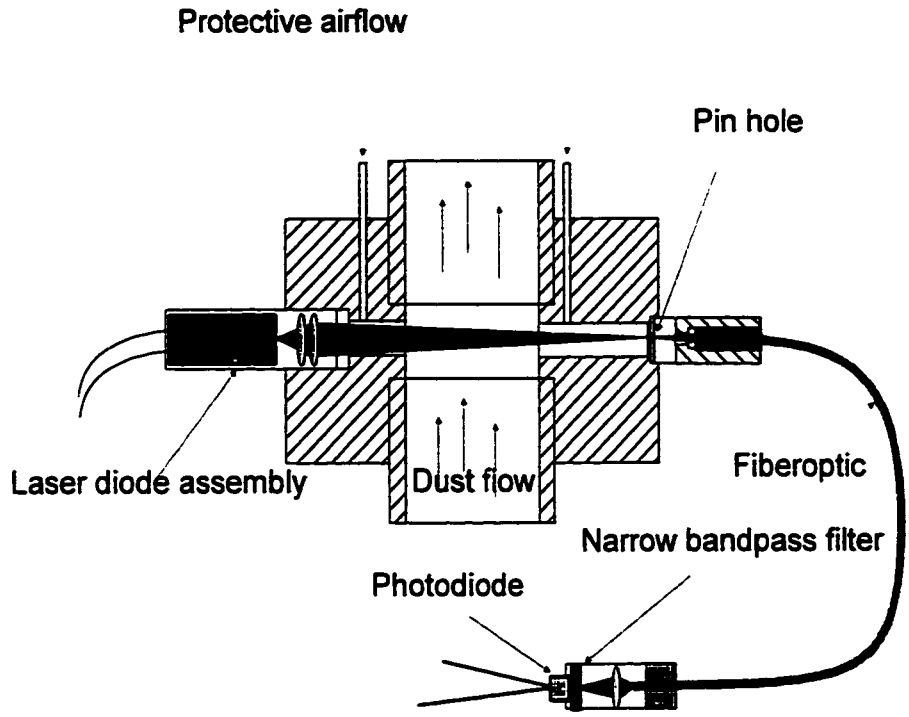

Figure 8: Close-up schematic of the optical dust concentration measuring setup (light extinctiometer).

The use of a built in optical measuring device enables light scattering to be at a minimum. Previously a laser beam was sent through a dust column upon exiting of the nozzle and passed underneath a cooling ring [16]. The laser beam now is protected and within the dust tube so that no outside light can interfere with the light attenuation signal. The light signal is first acquired by an oscilloscope for real time measurement and then sent to the PC data acquisition computer for data storage. The oscilloscope allows for a constant monitoring of the concentration and a guide for mixture control during an experimental burn.

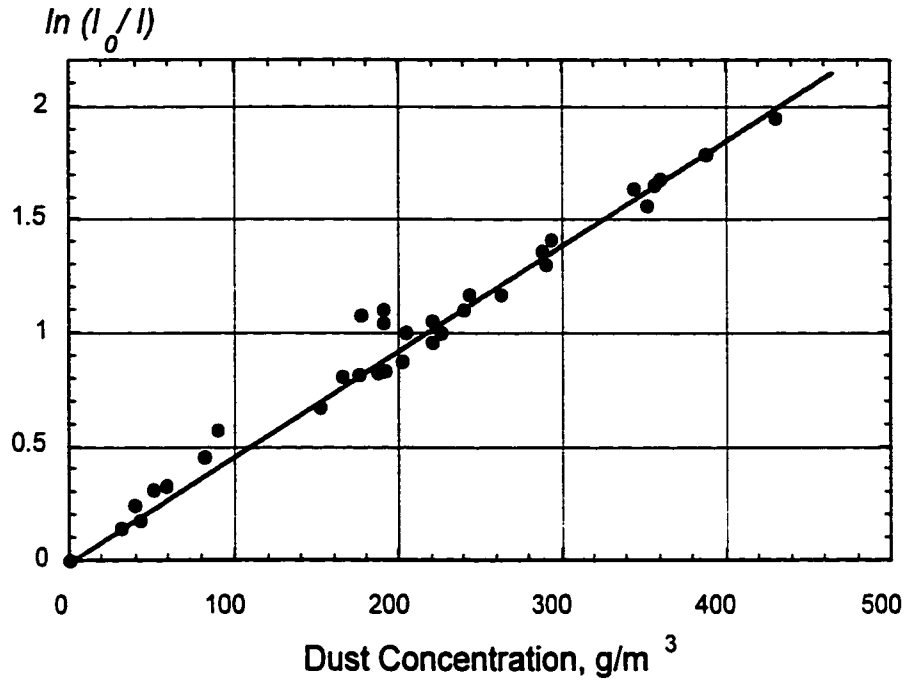

Figure 9: Calibration curve for the light extinctiometer.

Calculations for the estimated particle diameter (obtained through the light extinctiometer calibration data) are as follows. According to the Beer-Lambert law[17],

$$\ln\left\{\frac{I_o}{I}\right\} = kx$$

where **x** = the dust flow thickness (or tube diameter) and

k=slope of the calibration curve or;

$$k = Ns_o = \left\{\frac{B}{\frac{4}{3}\pi r^3}\right\}\left\{\frac{\pi r^2}{\rho}\right\}$$

where **N** =number of particles

s_o=Sauter cross section

B =dust concentration

r =particle radius

ρ=particle density

2.3 Aluminum powder

The dust that was used in the following experiments was atomized aluminum powder (Ampal 637, Ampal Inc., NJ). The powder used in these experiments was from the same batch as past experiments carried out on flame quenching distance measurements [13] and flame speed measurements in rich aluminum air mixtures [16]. Although many metallic powders are commercially available, aluminum was chosen for its relatively high reactivity, safe and easy storage, and important commercial and industrial significance. Within the aluminum powders' classification, many particle sizes are available. The average particle diameter range for commercially available aluminum is from the several nano-scale size to the several hundred microns size. The nano-scale particles are extremely reactive and very expensive. The several hundred micron size particles, although safe and inexpensive, are not easily ignitable in any concentration. Therefore, the 5 micron average particle size aluminum (Ampal 637), which was in the middle of the available particle size range, was chosen for the following experiments (for the sake of comparison and consistency of past experiments in aluminum powder combustion). The Ampal powder's aluminum content is no less than 99.5% and the aluminum particles are of a spheroidal or nodular shape [16]. Differential distribution of particle sizes in the powder can be seen in Fig. 10.

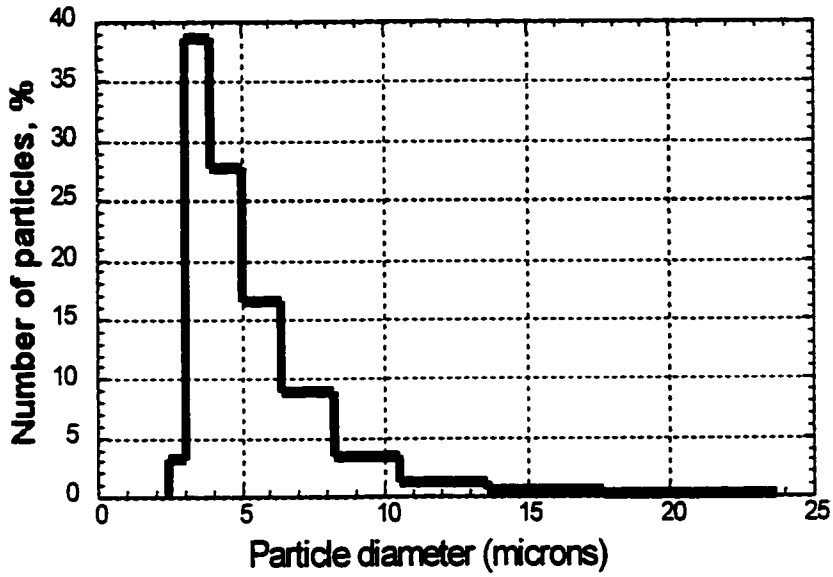

Figure 10: Particle size distribution in the Ampal 637 aluminum powder.

2.4 Photographic Arrangement

The flame image was split by a semitransparent mirror as is shown in Fig.11 and simultaneously recorded by two single-lens Canon reflex cameras through two different narrow bandwidth interference filters. The bandwidth of one filter coincides with the sodium D-line (589 nm) and the bandwidth of the other coincides with the edge of the green band in the aluminum oxide (AlO) molecular spectrum (508 nm). As the sodium concentration in flame remains constant, the maximum intensity in the sodium radiation might be associated with the maximum flame temperature [18], whereas the appearance of the AlO line indicates the ignition of aluminum particles[19]. The flame images were

digitized using a Nikon LS-2000 high-resolution slide and film scanner. The flame shapes and surface areas of the flame inner cones were determined with the help of image processing software. The previously used photographic setup was limited to simple gray filters and a single camera [15]. The modified setup now has two cameras taking simultaneous pictures through the above mentioned interference filters allowing us to have more detailed images of the dust flame and compare differently filtered images of the same flame.

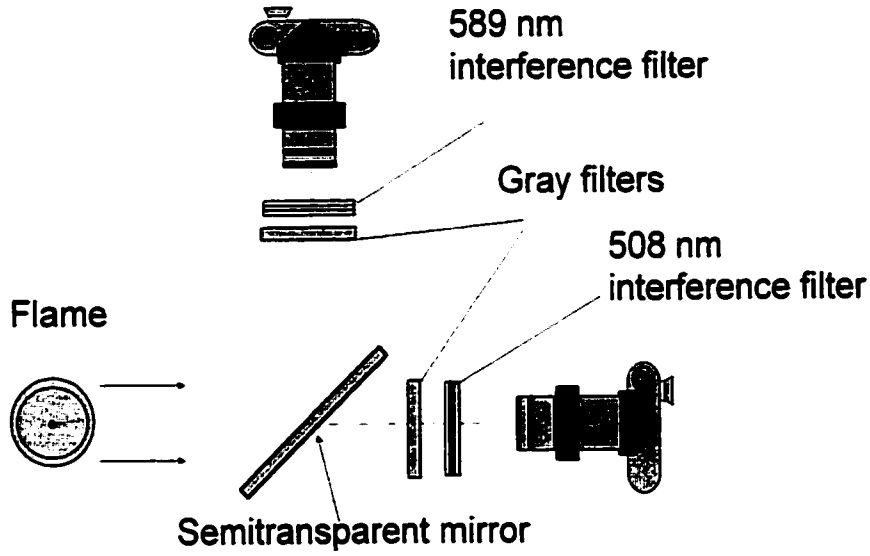

Figure 11: Schematic showing the photographic data acquisition layout.

The two cameras are linked by the same trigger cable so as to ensure simultaneous images. The cameras and the trigger cable are connected to the PC data acquisition computer and every picture taken is recorded as "spike" signal and is superimposed on the screen along with the dust concentration measurement. This enables the picture taken of the dust flame to be compared with the aluminum dust concentration at that time.

2.5 Typical Experimental Burn

An experimental burn on the dust burner is begun by heating and drying the dust sample that is to be burned. This is done by placing a sufficient quantity of sample dust within a pan-like container and placing it an electrically heated oven on a medium setting. This process is not crucial to an experiment but it has been found to facilitate the ignition and burn of the sample dust. By heating the dust, any moisture or "clumping" of dust can be avoided and easily handled afterwards. The dust is left to dry overnight, preferably, and then minutes before an experimental trial it can be placed in the dispersion piston.

The photographic cameras have to be loaded with the appropriate film and set at the desired distance from the flame to obtain a desired image. The data acquisition computer is turned on and a quick diagnosis of the light extinctiometer along with the oxygen analyzer is be performed. Once the electronics have been readied and the data acquisition started, the gas handling system is turned on. The dry-air bottle for the disperser valve and the co-flow valve are set to previously determined flows. At this point the ignition torch is opened and lit above the nozzle exit. As the dispersion piston is made to begin feeding of the dust to the tube, the quantity of dust can be monitored by the light extinctiometer using an oscilloscope. When the dust-air mixture is sufficiently rich, the ejector valve is turned on and fine-tuned, careful regulating of the dust flow enables ignition to take place. Once the ignition of the dust flow appears stable enough, the torch is shut off and the flame is seen settling down to the nozzle rim.

The ejector flow can be varied but the setting must be noted as this gives the value of extracted flow from the main disperser flow and thus the nozzle flow into the flame. At this point the concentration can also be varied from the piston feeding rate (potentiometer). Once the experimental parameters have been set, the cameras can be used and pictures taken. It is important to operate with safety welders' goggles as the dust flames are very bright and can be harmful if seen with the naked eye for too long period. The absence of drafts in the laboratory is also recommended. The products of the dust flames (mainly AlO) are vented above the burner through a fume hood as they are very fine and produce a dense white cloud. The fume hood should be the first and the last item to be operating during any experimental burn to ensure proper ventillation.

Figure 12: A photograph taken during a typical experimental burn.

Chapter 3
Observations

The lack of reliable burning velocity data in dust combustion has been accompanied by a lack experimental photography and images of dust flames. Many images of propagating dust flames have been obtained in the past but not much attention was give to the quality of these images. In Cassel's pioneering investigations of stabilized dust flames, much could be inferred from the images alone, (i.e. lifting of the flame base from the nozzle rim, flame tip curvature, particle flow behavior in a combustion zone, etc.). In the present experimental investigation, much attention was given to photographic data acquisition since the accuracy of the burning velocity data depends very much on the accuracy of the flame images. In addition to taking great care in obtaining clear flame pictures, various photographic techniques and image sampling methods were experimented with in order to obtain extra visual information from the flame images as possible.

The following chapter aims at giving a qualitative description of what was observed throughout the entire experimental investigation. Many phenomena such as flame curvature, flame lifting, blow-off and flashback will all be discussed as well as the various observations made in varying the experimental parameters such as flow rate, dust concentration and nozzle diameter.

3.1 The Bunsen Dust Flame

The figure below shows a typical stabilized aluminum dust flame. The stabilized dust flame has remained largely researched in the field of dust combustion. The lack of research carried out on Bunsen dust flames can be mainly attributed to the complexities involved building and running a dust burner. Since Cassel's report on dust flames in the early 1960's very few attempts in research were successful in reproducing his results. Even fewer graphical descriptions and photographic data exist on the Bunsen dust flame to give a general idea of what the phenomenon appears like. In the following chapter, a concise description of the stabilized aluminum dust flame will be given along with the methods used to obtain the dust flame images.

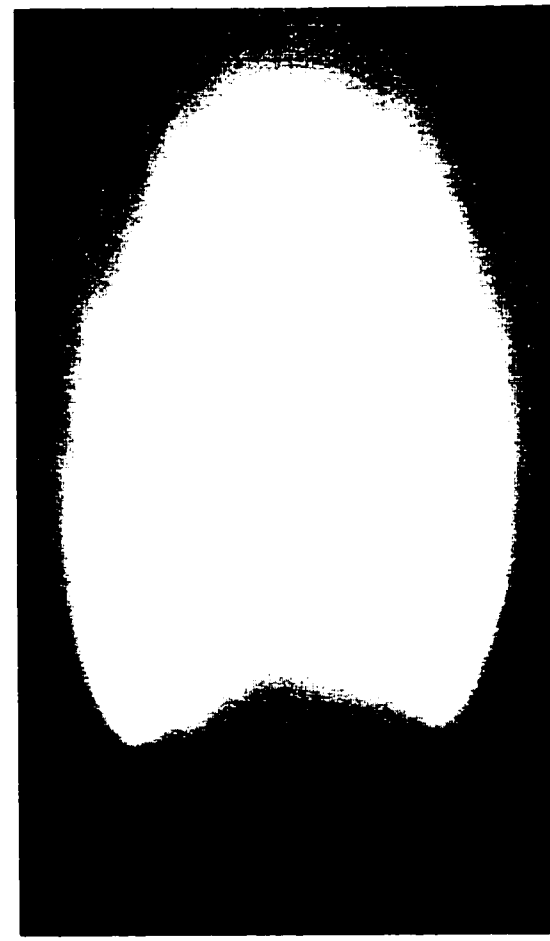

Figure 13: A stabilized aluminum dust flame on an 18mm diameter nozzle. The picture was taken with a neutral gelatin filter.

In Fig. 13, the aluminum Bunsen dust flame is shown stabilized on an 18 mm diameter nozzle. This picture was taken with a Fuji 100x color film, at 1/1000 exposure, using a simple Kodak gelatin neutral filter. The filter was used because of the dust flame's extremely bright nature. Careful observation of the picture reveals actual unburned aluminum dust flows (prior to entering the combustion zone at the rim of the nozzle). Further up on the tip of the flame (combustion product region), converging flows of aluminum oxide can also be seen exiting the flame region. If we observe and enlarge the area near the rim (Fig. 14), the dust flows can actually be seen bending around the nozzle exit forming the anchoring position of the flame.

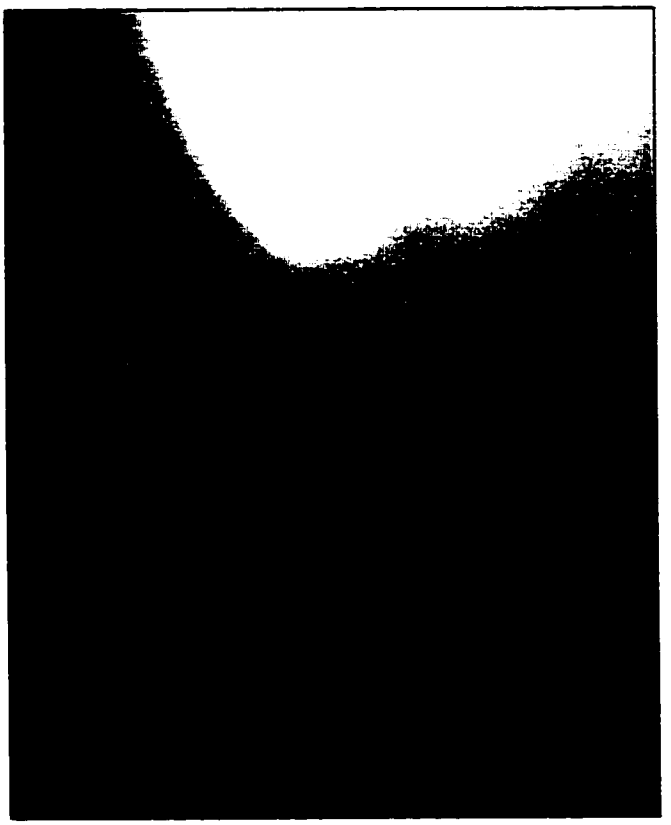

Figure 14: A close-up of the flame in figure 10. Note the curved stream that the unburned dust makes upon exiting the nozzle.

The flame in Fig. 13 is at a mixture composition of approximately 330 g/m^3 and exits the nozzle at a flow rate of 270 cm^3/s. Unfortunately, not much more can be seen of the flame without further addition of optical filters. Below are two comparison images of a methane flame and an aluminum dust flame. Fig. 15 shows the same flame using the same photographic film as Fig. 13. However, the camera was now equipped with a dense neutral filter, and the photograph was taken at an exposure of 1/30.

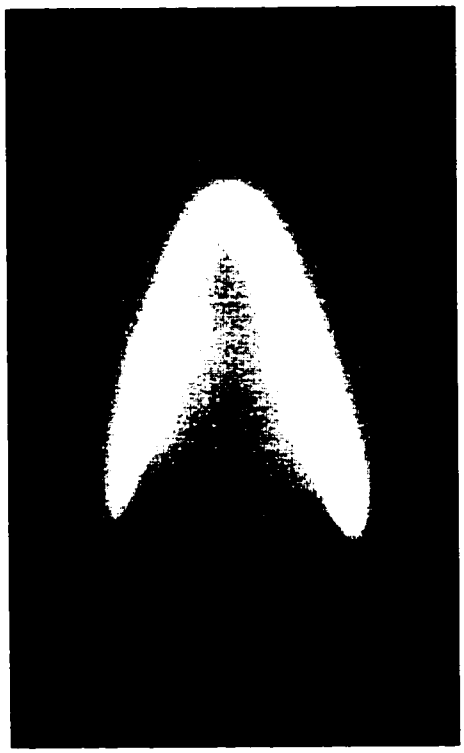

Figure 15: Aluminum-air flame stabilized on an 18mm nozzle. The aluminum dust-air concentration is 330g/m^3 (corresponding to ϕ=1).

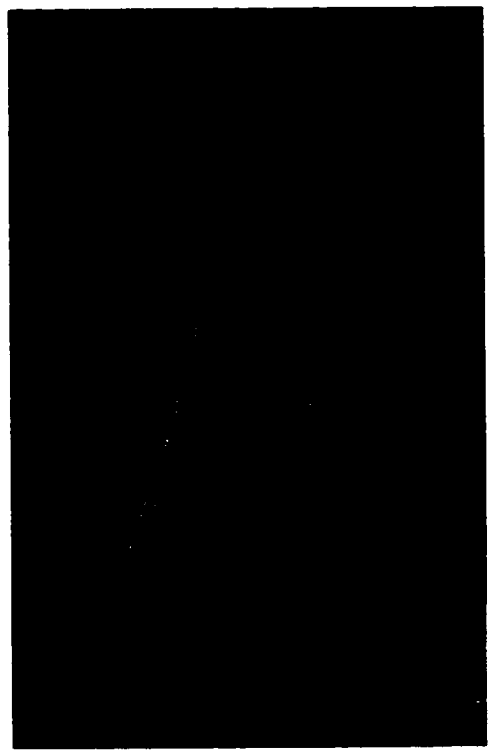

Figure 16: Methane-air flame stabilized on the dust burner apparatus with an 18mm nozzle. The mixture is 9.5% methane (corresponding to ϕ=1).

In Fig. 15, most of the flame's brightness has been filtered out and the presence of an inner cone can now be seen easily. With this image, further observations can be made with respect to the well-known Bunsen gas flame. The methane flame in Fig. 16, in comparison, was taken with Fuji color 1600x film with no optical filter; it too was taken at 1/30 exposure and with a fuel-air mixture 9.5% (stoichiometric) at a similar flow rate to the dust flame. In addition to being orders of magnitude brighter and radiating much more heat, the apparent flame thickness of the dust flame is several times larger than the methane flame. The inner boundary of the dust flame region is a lot sharper and more defined then the outer boundary, which appears undefined and diffuse. Possibly due to the much larger flame thickness, the Bunsen dust flame seems to also produce a larger tip curvature, when compared to the gas flame. The side shape of the gas flame also appears to be concave as opposed the straighter sides of the dust flame. As seen earlier, the flame base is also anchored at a much higher position than the methane flame and the anchoring of the dust flame base is closer to the inside of the nozzle rim. Unlike the methane flame, no overhang about the nozzle rim can be observed on the aluminum dust flame.

3.2 Optical Filter Observations

In experimenting with various optical filters, the dust flame images yielded more information. Narrow bandwidth photography of the dust flames, as described in the experimental setup, was used to observe and obtain data from the Bunsen dust flames. The first filter that was used was a 508 nm narrow bandwidth interference filter. This filter was used to try and obtain flame profiles of light that had a corresponding wavelength of the aluminum oxide molecular spectrum (the primary products of an aluminum-air combustion reaction). The 508 nm narrow bandwidth filter actually corresponded to the light emission of the upper edge in the aluminum oxide spectrum. This spectral data was obtained through previous experiments carried out on a typical dust flame as seen through neutral gray filters[19]. The other narrow bandwidth interference filter used was made for the 589 nm-wavelength region. This filter was chosen to permit the passage of light emitted from the flame to be in coincidence with the sodium D-line emission. As the sodium concentration in the flame was kept constant (by doping the aluminum powder samples with finely ground salt), the maximum intensity emitted in the sodium radiation could be associated with the maximum flame temperature. In the case of the 508nm-wavelength filter, the appearance of the aluminum oxide line indicates the ignition of aluminum particles and the reaction front position.

The main objective behind this dual filter photographic investigation was to observe any difference in the aluminum dust flame profiles. Both flame images were scanned and digitized using a Nikon LS-2000 high-resolution slide-film scanner. In many cases, the profiles that were seen through the aluminum oxide and sodium line optical

filters yielded flame profiles that were more or less coincident to one another. However, when flame pictures of stoichiometric dust-air mixtures were analyzed (330 g/m^3) the aluminum oxide and sodium line flame profiles showed less coincidence and a small discrepancy was found between both profiles when superimposed. The difference in the superimposed images was noticeable at a small region near the tips of the flames (Fig.17).

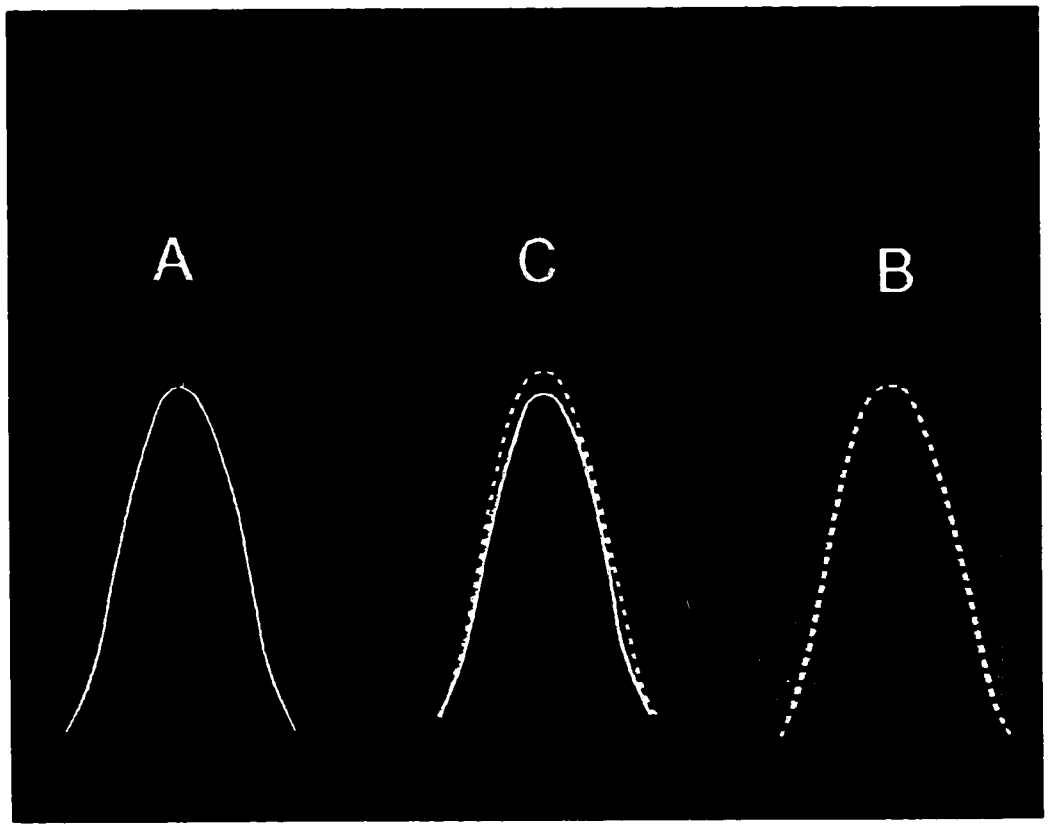

Figure 17: Aluminum dust flame seen through a 508nm (A) and a 589nm (B) narrow bandwidth interference filters. Superimposed contours of the inner flame cones is shown in the center figure (C).

It is interesting to note that other observations can be made from the images of the two different optical filters. In Fig. 17, the flame representing part of the aluminum oxide spectrum (seen to the left in green) does not show light beyond the diffuse boundary of the conical flame. The flame image representing the sodium D-line (seen to the right in yellow) however clearly shows more light emitted from the same flame. The streamlined contour flowing from the flame in a plume-like manner is very clear in the image taken with the sodium D-line interference filter. Because of the excess light that was present in the sodium D-line flame images and the faint differences in profiles when compared to the aluminum oxide flame images, only aluminum oxide and neutral optical filter images will be discussed for the remainder of the present work.

3.3 Dust Concentration

The recent experiments that were conducted concentrated on the effects that certain fundamental parameters might have on the Bunsen dust flame. The first experimental observations involved the variation in dust-air concentrations. Using an 18 mm nozzle and a constant flow rate, a range of stable flames in dust concentrations from 200 g/m^3 to 600 g/m^3 was obtained. Knowing the flow rates and flame surface areas (which were calculated through revolution of the flame profiles) burning velocities could be calculated, as described by Andrews and Bradley [20]. The flames yielded an average burning velocity of 15 cm/s to 20 cm/s over a wide range of mixture ratios; in other words, the burning velocity displayed little or no dependence on the dust concentration. The dust flows were only ignitable in the rich mixture regime, after which a flame was stabilized on the nozzle rim. Once a stable flame was obtained the dust-air mixture composition was varied, meanwhile maintaining a constant flow rate. As the concentration was varied, a visible variation in the size of the dust flames was barely noticeable; however, the variation in brightness or luminosity was much more apparent.

The flames ranging from lean to stoichiometric (200 g/m^3 to 300 g/m^3) were characterized by a bright white color (Fig.18). The usual dust flame characteristics, as described earlier, were apparent in the lean aluminum dust flames. The flame thickness was very luminous and several times wider than a gas flame. The inner flame profiles were very distinct surrounded by a diffuse outer boundary. At the base, the flame would begin either on the burner rim or slightly within the nozzle. It would curve slightly (producing a rounded flame base) and then gradually straighten out to form the slanted

side of the cone similar to the methane flame. As the transition from a lean to rich mixture progressed (ie. concentrations in the range of 300 g/m^3 to 350 g/m^3), an interesting observation could be made when seen with color film. The flames still had a conical shape with the white colored boundary surrounding them, but the flame tip was, in many cases, a distinct mix of yellow and orange, similar to the general color of rich flames (Fig.19).

The richer flames (350 g/m^3 to 600 g/m^3) were slightly larger in thickness than the lean flames and were slightly shorter in flame height (Fig. 20). The inner cone was also very distinct with a rounded tip, and the flame was surrounded by the diffuse outer boundary profile. The flame was, however, much brighter and characterized by a mix of bright yellow and orange color. Another observable difference was in the bright outer region that was formed around the main flame. This outer region was in the shape of a contoured flow tapering in a "tear drop"-like shape downstream of the flame. A thin bright zone (resembling a secondary combustion region) that diminishes in intensity as it travels downstream characterizes the base of this region. Both lean and rich flames showed a similar elevation over the burner rim, which was several millimeters in height. All three figures (Figs. 18, 19 and 20) were taken with dense neutral filters and Fuji 100x color film.

Another interesting observation was the existence of such phenomenon as open tip flames, as has been recorded in the past for stable gas flames[20]. This condition was reached when the mixture was too rich (in excess of 600 g/m^3). In Fig. 21, the flame's tip is slightly opened and the image was taken with a the 508 nm interference filter and Fuji 100x color film. Flashbacks and blow-off were both observed in the present work.

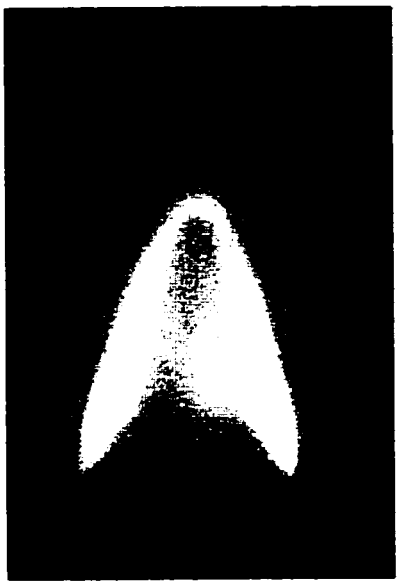

Figure 18: Aluminum-air flame stabilized on an 18mm nozzle. The dust-air concentration is 270 g/m^3.

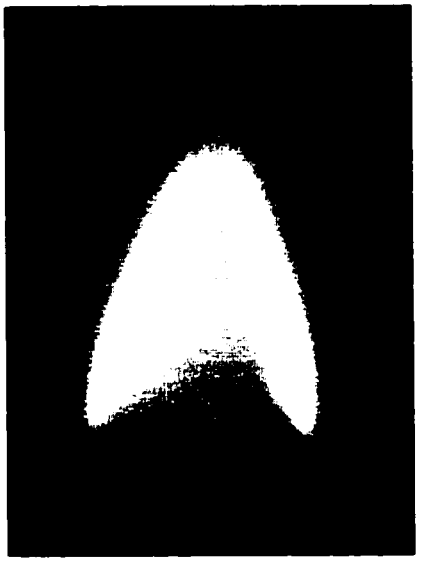

Figure 19: An aluminum-air flame transitioning from a lean to a rich mixture (stoichiometric, 330g/m^3). Note the yellow color in the tip region of the flame.

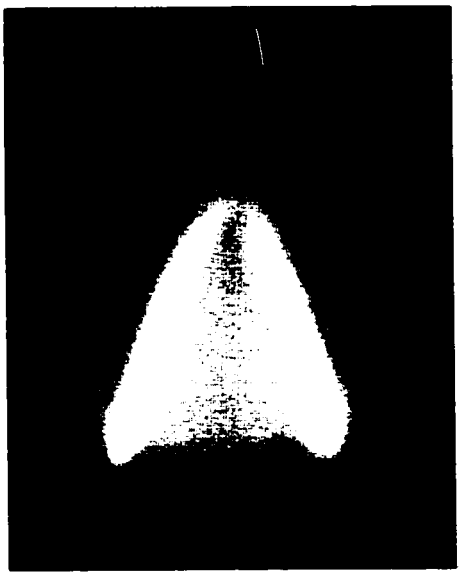

Figure 20: An aluminum-air flame stabilized on the same 18mm nozzle however, rich in mixture composition (550 g/m^3). Note the luminous contours flowing upward from the flame base.

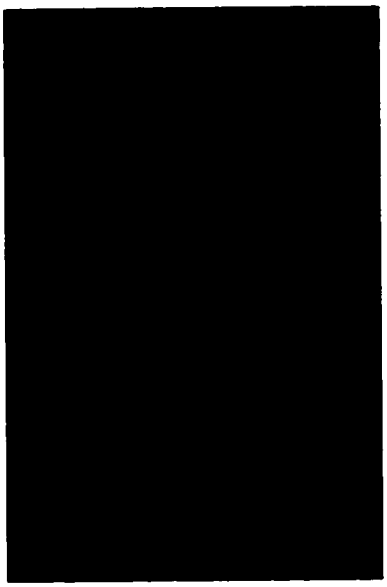

Figure 21: Example of an open tip flame seen with the 508nm interference filter.

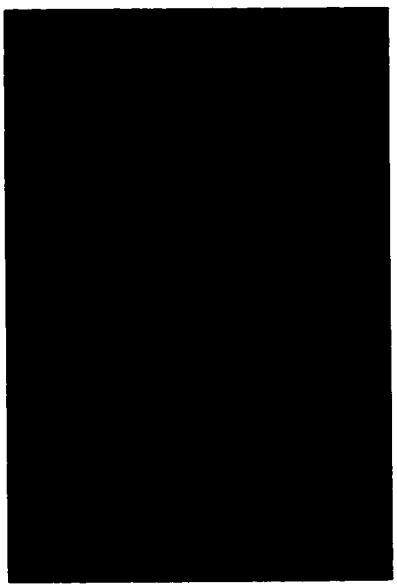

Figure 22: Blow-off of an aluminum-air flame, seen with the 508nm interference filter.

Of the two phenomena of flame limits, the blow-off condition was the only one recorded on film. The flashbacks, although accidentally occurring from time to time, were generally avoided because they had the potential to damage the inner burner tube. The image in Fig. 22 was taken with the same method and equipment as was used in Fig. 21. The mixture limit at which a dust flame was no longer stable in the fuel lean regime was at a mixture composition of approximately 180g/m^3. Flames that were stabilized below this limit could not be categorized as stable. Flames stabilized beyond this point would not have a continuous surface but rather a part of it "missing" or perforated (Fig.23). This perforation would usually occur at the base (although some pictures show perforations on the sides of the cone) and sometimes the perforations were seen travelling in a circular fashion around the rim before quenching or extinguishing the flame.

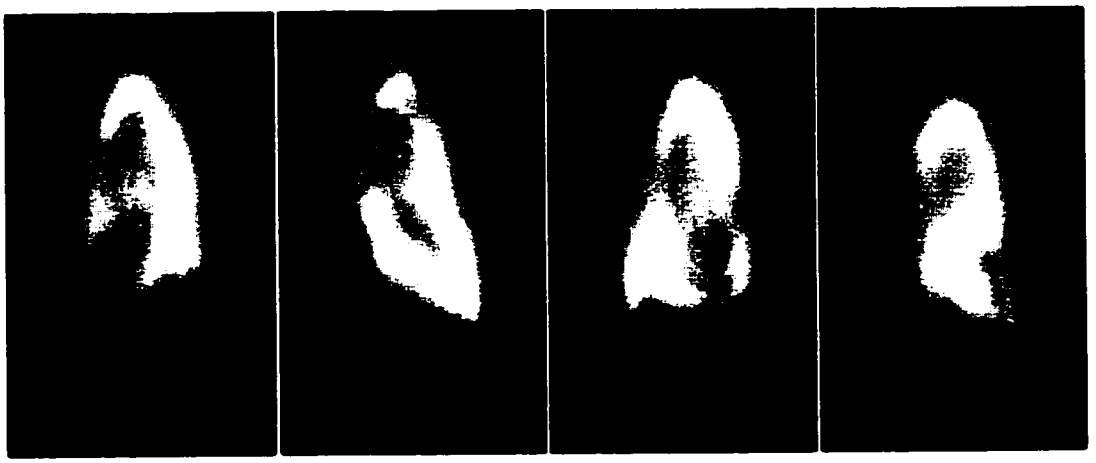

Figure 23: Successive images of an unstable lean aluminum dust flame. The mixture composition is less than 180 g/m^3. The detached flame base can be clearly seen.

3.4 Flow Rate

The next parameter to be experimented with was flow rate variation. As before, a flame was stabilized at a given flow rate and then fixed. As the dust-air flow rates were increased and dust concentrations varied along the same range that was mentioned in the previous sections (200 g/m^3 to 600 g/m^3) the burning velocities obtained were now higher, 20 cm/s to 27 cm/s. Visibly, the difference between the higher flow rate flames and the lower flow rate flames was in the slight lifting of the flame base (no more than a few millimeters) and the increase in flame surface area. The increase in surface area, however, was not in proportion to the increase in flow rate. In other words a two-fold increase in flow rate did not yield a two-fold increase in surface area, as can be observed in pre-mixed

gas flames. This peculiarity, therefore, yielded the higher burning velocities. Another visible difference between the higher flow rate flames and the lower flow rate flames was in their tip curvature. The taller and higher flow rate flames had a much smaller dome shaped tip in comparison to the shorter and lower flow rate flames which formed a large dome shaped tip with large curvature. The flame thickness, however, did not appear to be altered by the variation in flow rate. In Fig. 24, the comparison of various flames at different flow rates can be made

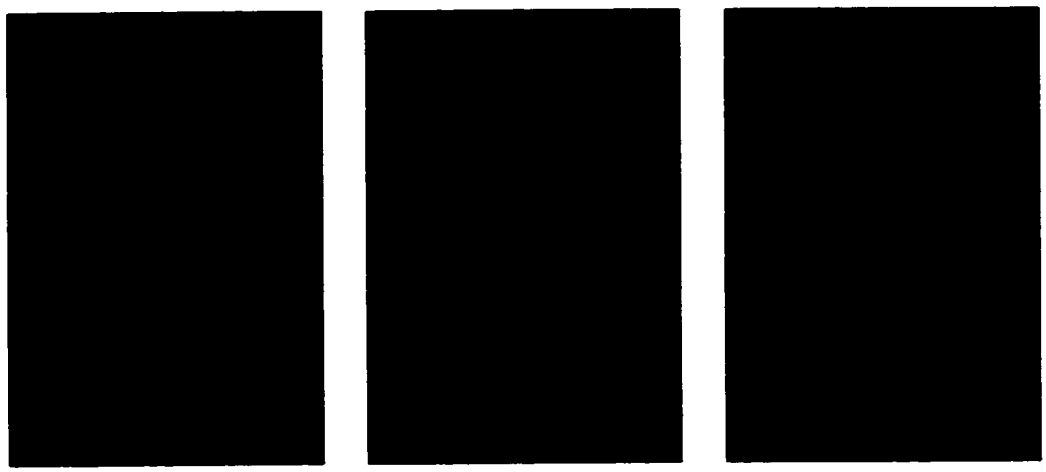

Figure 24: Stabilized aluminum dust flames on an 18mm nozzle at different flow rates seen with the 508nm interference filter.The flow rates are, from left to right, 180cm^3/s, 270cm^3/s and 320cm^3/s.

3.5 Nozzle Diameter

The experiments were then repeated for a smaller nozzle (14 mm diameter) and both variations in mixture composition and flow rate were experimented (Fig. 25). The characteristics of the 14 mm nozzle dust flame did not differ much from the 18mm nozzle flame. The flames were stabilized within the same range of concentration as the 18 mm nozzle flames and the same range of flow rates. Although the 14 mm nozzle diameter was a 40% decrease in cross sectional area from the 18mm nozzle, the reduction in flame surface area was a mere 10%. This in turn yielded higher average burning velocities in the 14 mm nozzle by approximately 20%.

When the experiments were carried out on the 21 mm nozzle, the reverse conditions were observed. The 40% increase in cross sectional area of the nozzle gave nearly 130% increase in flame surface area but only a 10% decrease in burning velocity. The large nozzle flames, however, were not stabilized at the same flow rates that the 14 mm and 18 mm nozzle flames were stabilized at. In fact the lowest flow rate that the large nozzle flames were stable at (before producing flashback) was approximately 100 cm^3/s higher than the highest flow rates for the 14 mm and 18 mm nozzle flames. In other words, for the large nozzle, flashback would occur easily at less than 400 cm^3/s. Flashback, for all nozzle sizes experimented with, was first noticeable on the nozzle rim, where the flame would cease to be anchored and begin to travel downward within the nozzle. The larger nozzle flames differed in base elevation from the smaller nozzle flames in that they were generally lifted off a few millimeters higher (or greater in some cases)

Figure 25: Effect in aluminum dust flame geometry with nozzle diameter. The flame are seen with a 508nm interference filter at similar concentrations (550 g/m^3) and flow rates (400cm^3/s). The flames are stabilized on different nozzles, from left to right, 14mm, 18mm and 21mm.

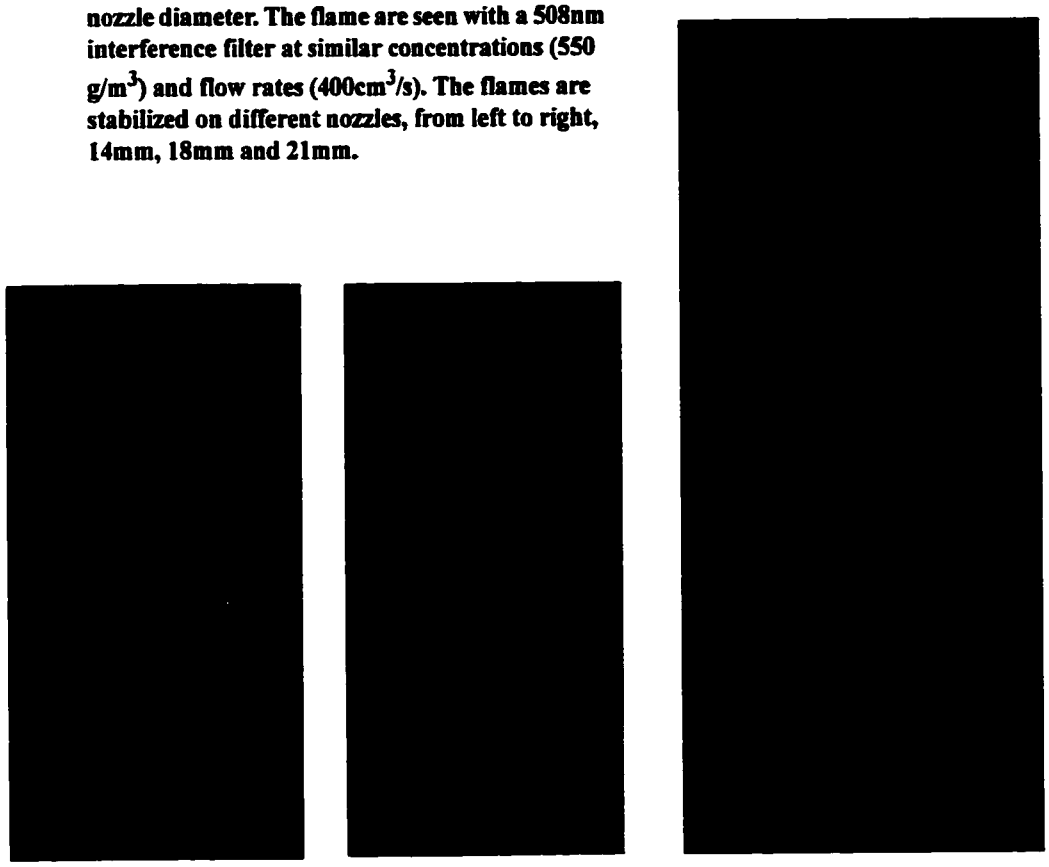

than all the other flames. The inner part of the large flames was not so distinct as the smaller flames. The flame profile for the large nozzle resembled more to that of the classical Poiseuille flow profile than the typical cone that was observed in the earlier smaller flames. The tip curvature was however similar to the smaller flames and the apparent flame width was also similar but not as smooth as the smaller flames.

This variation in burning velocities with varying nozzle diameter was also observed by Cassel in his early experiments. But not much photographic data was obtained to show the detailed structure of the dust flame and the dust burner was never validated as a reliable means by which to measure burning velocities. In the recent experiments, great care was taken to ensure that the photographic data was extensive and detailed. Some data and photographic work was also carried out on methane flames to give the possibility of comparison to aluminum dust flames as well as to verify the reliability of the dust burner as a valid experimental tool by reproducing known data with premixed gas flames.

Chapter 4
Results and Discussion

The means by which the burning velocities was obtained in the present work was by the method of flow rate and flame surface area as discussed by Andrews and Bradley. This method has been used extensively by many researchers in the field of stabilized gas flames in obtaining accurate burning velocity measurements. However, as first discussed by Markstein, flame curvature proved to be a significant factor that needed to be taken into account when calculating burning velocities of stabilized gas flames. This phenomenological effect was considered in the present investigation and applied to the stabilized aluminum dust flames.

The following chapter will discuss the experimental trends that the aluminum dust flame burning velocities exhibited when the various parameters of dust concentration, flow rate and nozzle diameter were varied. Subsequently, the topic of two-phase flow will be addressed briefly followed by a discussion of dust flame structure (flame thickness in dust flames) as well as the effect of flame curvature on stable dust flames.

4.1 Experimental Results

Burning velocity measurements were taken by means of the total surface area and flow rate method as described by Andrews and Bradley[20]. There was generally very little difference of the inner cone profile in flame pictures taken with the 508 nm filter or the 589 nm filter. Since the 508 nm filter corresponded to the approximate position of the reaction front, it was decided to use only the 508 nm filter images for the use of inner cone profiles. The images were then scanned directly from negative filmstrips and the inner cone profiles were plotted as curves. The curves were then revolved through a complete 360-degree turn producing a three-dimensional cone image. The image was then analyzed through design software and a surface area was then obtainable. The flow rates were obtained from rotameter measurements and taken directly from the apparatus. Dividing the nozzle exit flow rate by the flame's surface area gave the burning velocity.

The present experiments confirm the result of previous work carried out on the same apparatus, using an 18 mm brass nozzle, by Goroshin et al [16] which was able to demonstrate that flame speeds in rich aluminum-air dust suspensions are generally insensitive to dust concentration. In other words, a wide plateau-like region can be seen for a wide range of mixture composition yielding an average burning velocity. However, the average burning velocities obtained in earlier work by Goroshin et al. were higher than the present work. It is interesting to note that the measurements obtained also show no observable decrease in burning velocity when the flames are stabilized in the range of dust concentrations below stoichiometry (i.e. lean aluminum-air mixtures from 200 g/m^3 to 300 g/m^3). Although flames slightly below the 200 g/m^3 limit were observed, for reasons

of instability (as described in Chapter 3) they were not used in burning velocity data. In the fundamental report on stabilized aluminum flames by Cassel [14], flames of much leaner concentrations than 200 g/m^3 were obtained. Although the present work was not able to reproduce such lean flames, much lower burning velocities were, in general, obtained compared to Cassel's work.

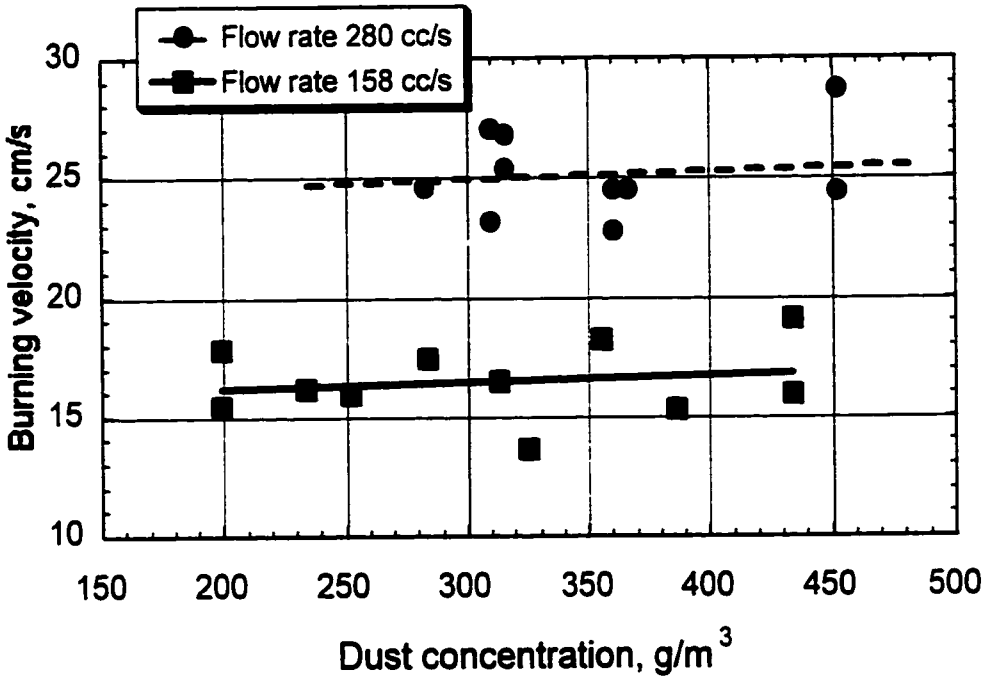

Figure 26: Dependence of burning velocity on concentration at two different flow rates using an 18 mm nozzle.

Past work by Cassel, and Goroshin and Lee on stabilized aluminum flames did not observe any dependence of burning velocity on flow rates[14][16]. Burning velocity data for the 18 mm nozzle was obtained through a range of concentrations as well as flow rates. In Fig. 26, two flow rates were experimented with and the general trend of the plateau-like curve is still visible. At a flow rate of 158 cc/s, an average burning velocity of approximately 16 cm/s was found. When the flow rate was increased to 280 cc/s, the average burning velocity increased to 25 cm/s for approximately the same range of dust concentration. The higher flow rate burning velocity data was not observable below dust concentrations of 270 g/m^3 due to the same instabilities that were described earlier in Chapter 3.

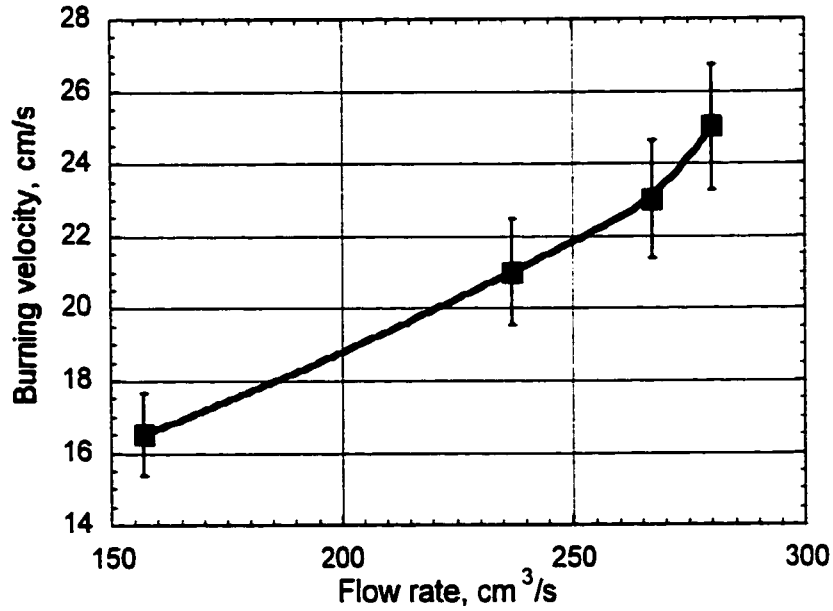

Figure 27: Dependence of burning velocity on flow rate.The dust concentration was kept at approximately 350 g/m^3 and flames stabilized on an 18mm nozzle.

The burning velocity, however, exhibited a clear tendency to increase with an increase in flow rate. The observed dependence of the burning velocity on the flow rate, at approximately uniform dust concentration (350 g/m^3), can be seen in Fig. 27. The apparent maximum flow rate at which the flame ceases to be completely anchored to the nozzle rim or exit, prior to blowoff, is approximately 300 cm^3/s, whereas at a flow rate below 150 cm^3/s the flame is prone to flashback. A flame stabilized on a low flow setting is short in height and exhibits a very round tip (large curvature) but as the flow is increased the flame increases in height and the tip curvature becomes less round; that is, the flame has a more acute conical tip. As the flow rate is increased, the flame tip loses the large curvature and transforms into a sharper cone-like form, thereby losing surface area and therefore causing an increase in the burning velocity. In other words, the flame's curvature responds dramatically to the changes in flow rate.

Other cylindrical brass nozzles that were used to stabilize the aluminum dust flames were constructed with the following exit diameters 14 mm and 21 mm. For these nozzles, aluminum dust flames were also stabilized at various flow rates to investigate the effects, if any, on the burning velocity. All of the nozzles experimented with have the same base diameter (25 mm) and height (60 mm). In the experiments carried out with varying nozzle diameters, it was not found to be possible to stabilize flames on the large nozzle (21 mm diameter) at the same low flow rates as on the 14 mm and 18 mm nozzles. For the 14 mm and 18 mm nozzles, stable flames were observed in the same flow rate range. The data shown in Fig. 28, displays burning velocities for similar flow rates using the two nozzle diameters of 14 mm and 18 mm and a flow rate of approximately 280 cm^3/s.

Interestingly, the lowest flow rate yielding a stable flame for the 22 mm diameter nozzle is much higher (approximately 400 cm^3/s). Nevertheless, the results clearly demonstrate that the burning velocity apparently decreases with increasing nozzle diameter. Cassel also reported similar observations in his experiments with Bunsen dust flames[14].

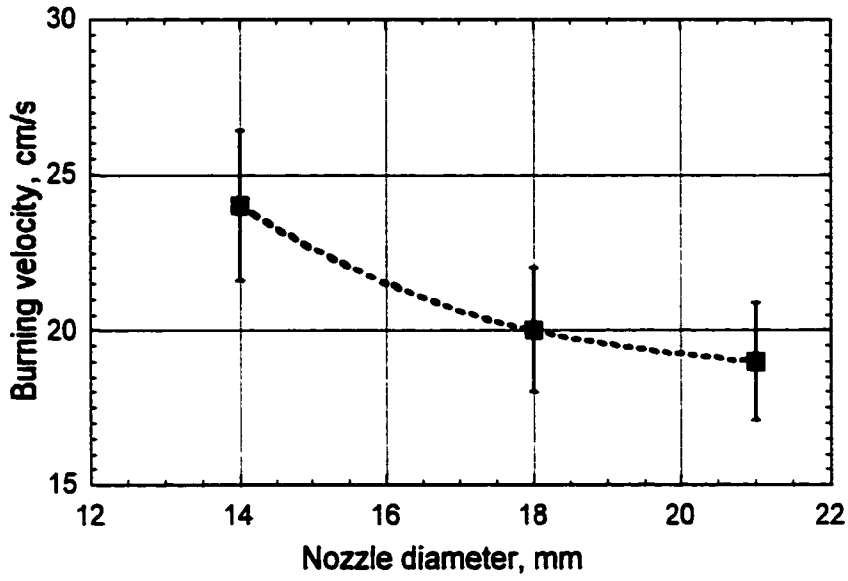

Figure 28: Dependence of the burning velocity on the nozzle diameter.

4.2 Two-Phase Flow

Since dust flows are hydrodynamically very different from gas flames, they can be expected to yield very different profiles and behaviors. If one were to consider particle inertia, it can be easily seen that the dust particles at the rim of the nozzle will not follow the gas flow around the bend in a quasi 90-degree flow pattern. In fact, the aluminum particles will tend to flow upwards due to their own momentum and not follow the same streamtubes that the gas flow creates. This would make it so that the rim of the nozzle would have a significant "dead-zone," void of aluminum particles where no combustion could take place due to an absence of fuel. This might help explain why such a noticeable flame detachment was observed on stable dust flames compared to gas flame detachment from the nozzle rim which can be less than 1mm. In addition to the hydrodynamics of dust flows explaining the flame lifting, there is the heat loss mechanism that should be considered. The height at which the aluminum dust flame is lifted from its base is approximately 3 mm and, as stated earlier, this is comparable to quenching distances obtained for aluminum-air propagating flame experiments.

If we consider the tip region of the dust flame, again considering particle inertia, we would have a higher concentration of aluminum since the particles would resist being diverted by the combustion wave. Another event occurring in the flame tip region is the divergence of oxygen by the lateral combustion zone (selective diffusion), creating a lack of oxidizer and an excess of fuel and thus enhancing the effect of a very rich tip region[18]. Open tip flames can be easily observed as shown in Chapter 3 where the flame is rich in aluminum dust concentration. However, another observation can be seen if the

flame is lean, a locally rich region will exist at the flame tip. A rich flame can be readily identified by its bright orange and yellowish color, whereas a lean flame is pale white in appearance. In some instances a flame may be laterally lean (white in appearance) but rich in mixture composition at the tip (yellowish in color).

4.3 Flame Curvature

In studying burning velocities of gaseous flames, it was found necessary to address the problem of relating the local burning velocities of a curved flame front to the flame flow field within the reaction zone region and the shape of the flame itself. Various attempts were made in the past to propose solutions to the above mentioned problem by addressing such issues as non-steady flow phenomena, chemical reactions and various transport processes that occur within the region of the flame front. All of these issues required very complex mathematical solutions therefore, many assumptions were made in order to bring forth slightly more simplified solutions.

The simplest solution, addressing the stability of flames, was that of a constant burning velocity, $S_u = S_u^o$, which was first proposed by Landau and Darrieus [21][22]. However, further experimental results later contradicted Landau and Darrieus, after which Markstein [23] presented a solution showing the dependence of burning velocity on flame curvature. The proposed curvature term was assumed to account for heat conduction and selective diffusion. Therefore Markstein's assumption, from an analysis of a two-

dimensional flame front, was presented in the following simplified form shown as equation (1)[24],

$$S_u = S_u^{\,o}\left\{1 + \frac{\mathcal{L}}{R_{flame}}\right\} \qquad (1)$$

where $\mathcal{L}$ is the characteristic length (thickness of the flame) and R_{flame} is the radius of curvature of the flame. In the case of $\mathcal{L}$, Markstein assumed that it was directly related to the thermal length L_{th} multiplied by a factor u ($\mathcal{L}=\mu L_{th}$). However, Markstein showed that if the Lewis number was equal to 1 and if selective diffusion was neglected, the parameter μ was also equal to 1 and therefore $\mathcal{L}=L_{th}$.

4.4 Dust Flame Structure

Cassel suggested [14] that the increase in the burning velocity for dust flames stabilized on smaller nozzles might be the result of the converging heat flux produced by flame curvature. Cassel speculated that due to the larger thickness of the dust flame, compared to the gas flame, the dust flame burning velocity might be affected even with a relatively small flame curvature.

The width of hydrocarbon flames is typically less than 1 mm and is dominated by the flame's preheat zone (also known as the Markstein length). Due to the strong Arrhenius dependence of the reaction rate on temperature, the reaction zone in gas flames occupies only a small temperature interval below the adiabatic flame temperature.

Therefore, the spatial thickness of the reaction zone in gas flames is negligible in comparison to the preheat zone. Unlike gas combustion, the combustion rate of dust particles after ignition is not controlled by Arhenius kinetics, but rather, is limited by the rate of oxygen diffusion towards the particle's surface. The average flame temperature has little effect on the diffusion-controlled combustion rate. Thus the reaction zone in dust flames occupies a wide temperature interval that spans from the particle ignition temperature (about 2200 K for aluminum particles) up to the adiabatic flame temperature (3500 K for the stoichiometric aluminum-air mixtures). Consequently, the spatial width of the dust flame combustion zone might be comparable or even exceed the width of the preheat zone (Markstein length) and the total width of the dust flame can be considered as a sum of the preheat zone and the combustion zone, in other words $\delta = \delta_p + \delta_c$ (Fig. 29). Therefore, even if we consider the Markstein lengths of the dust and gas flames to be similar (comparable flame speeds), the total thickness of the dust flame is larger.

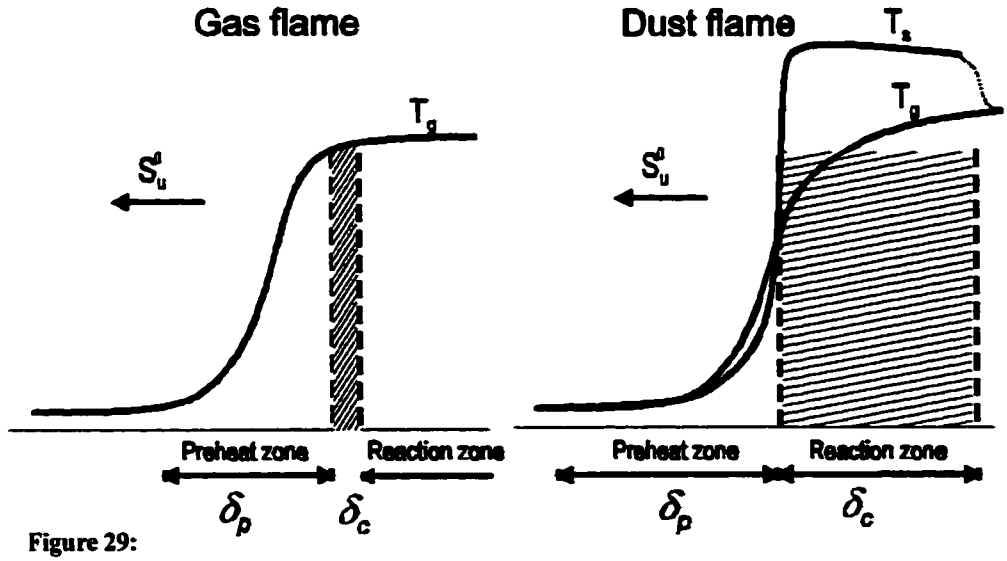

Figure 29: **Illustration of the flame thickness of a gas flame compared to the proposed flame thickness of a dust flame. Here, T_s is the particle temperature, T_g is the gas temperature and S_u^0 is the unperturbed burning velocity.**

The thickness of the aluminum dust flame can be estimated from quenching distance data. Flame quenching distances in aluminum-air suspensions have been measured by Goroshin and Lee [13] using the same aluminum dust as in the present experiments. It was found that the quenching distance in fuel-rich aluminum-air mixtures is about 5 mm and was found to have no dependence on the dust concentration. The simple flame quenching theory proposed by the authors in the same work [13] predicts the ratio of the quenching distance to flame thickness to be about 1.8 for aluminum dust flames. Thus, the estimated flame thickness of the rich aluminum dust flame is about 2.8 mm with at least half of this length belonging to the combustion zone, as explained earlier. We can now use the estimated flame thickness to calculate the burning velocity of the unperturbed flat flame S_u^o in accordance with the Markstein correction equation:

$$S_u^{\,o} = \frac{S_u}{\bar{A}} \qquad \text{where} \qquad \bar{A} = \overline{\left\{1 + \frac{\delta}{R_{flame}}\right\}} \tag{2}$$

Here S_u is the burning velocity of the Bunsen dust flame calculated by dividing the dust flow through the nozzle by the total flame surface area. The parameter $\bar{A}$ is an average value of the flame thickness-to-flame radius ratio calculated separately for each flame shape. The radius of curvature consisted of the normal distance from the axis of the flame cone to the surface. It was averaged with "weighted" radius which is proportional to the ratio of the dust flowing through the flame segment of the given radius to the total dust flow through the burner:

$$\overline{\frac{1}{R_{flame}}} = \frac{1}{H_o}\int_0^{H_o} \frac{1}{r(h)}\left\{\frac{r(h)}{R_o}\right\}^2 dh \tag{3}$$

Here H_0 is the flame height, R_0 is the radius of the flame base, and *r(h)* is the second degree polynomial approximating the flame profile. Several flame profiles that represent different nozzle diameters and flow rates were carefully measured to calculate average values of the parameter $\overline{A}$ along the flame height. The calculated burning velocity results of the unperturbed flat flame S_u^0 (in accordance to the expression in equation 1) are shown in Table 2.

Concentration g/m^3 ($\pm$ 50 g/m^3)	Nozzle Diam. mm	Flow Rate l/s	Flame height mm	S_u° cm/s
550	14	0.18	20	19.5
550	14	0.22	24	19.4
550	14	0.24	29	17.6
660	14	0.27	30	20.8
660	14	0.32	34	19.6
430	18	0.16	23	16.2
460	18	0.16	24	15.8
462	18	0.20	26	18.0
480	18	0.24	27	18.9
570	18	0.23	28	16.3
600	21	0.46	53	15.8
600	21	0.47	38	18.9
550	21	0.51	49	16.9
550	21	0.55	47	19.1
600	21	0.59	56	18.1
				S_u° = 18.1±1.3cm/s

Table 2: Curvature Corrected Burning Velocities

As can be seen from the Table 2 and Figs. 30, 31 and 31, the unperturbed burning velocity is largely independent on both flow rate and nozzle diameter. Hence the previously observed scatter of the non-corrected burning velocities is simply an artifact of the dust flame curvature effect.

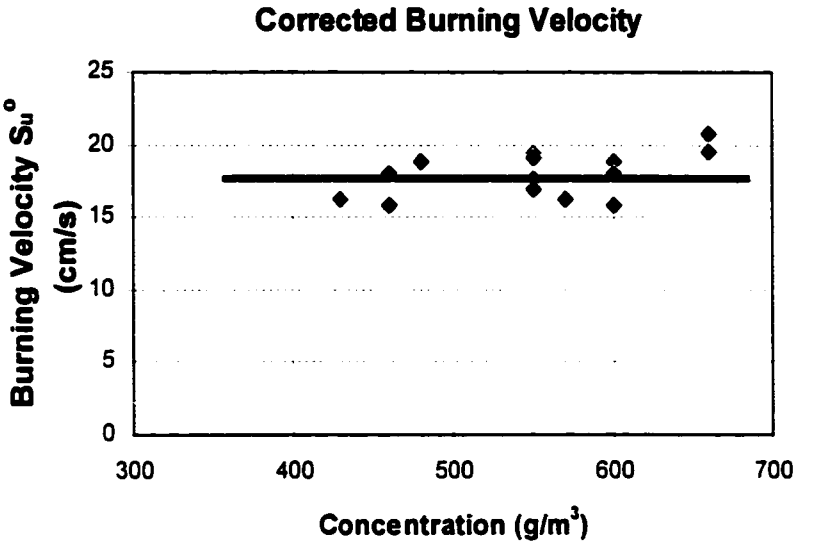

Figure 30: Corrected burning velocity dependence on the aluminum dust concentration.

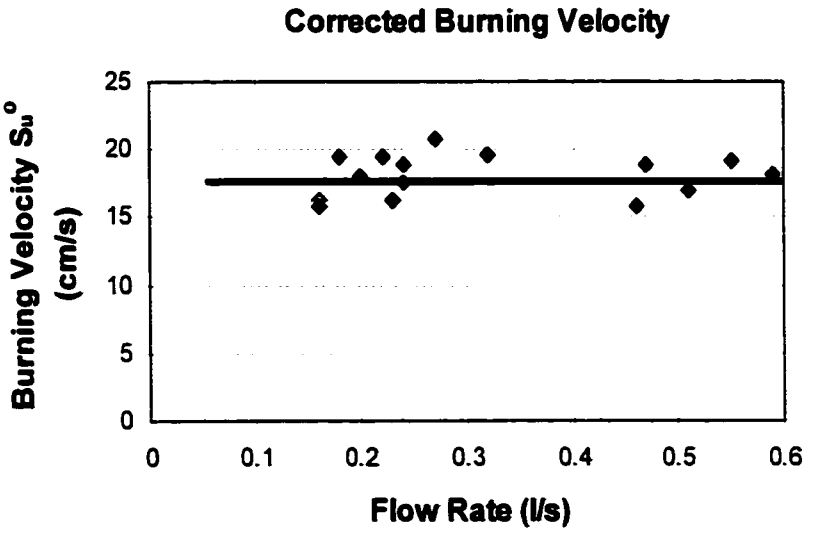

Figure 31: Corrected burning velocity dependence on the dust-air flow rate.

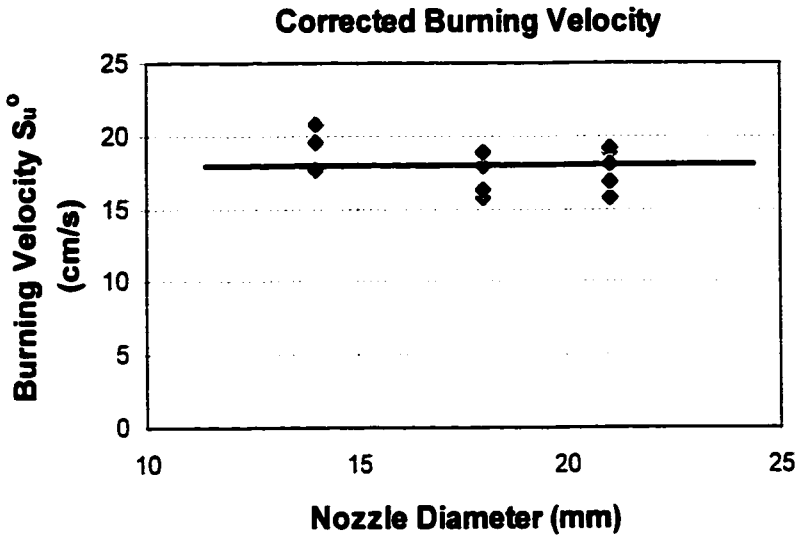

Figure 32: Corrected burning velocity dependence on the nozzle diameter.

Chapter 5
Conclusions and Recommendations

5.1 Conclusions

The laminar burning velocity of stabilized aluminum-air suspensions was studied experimentally in the present work. The aluminum dust flame was stabilized on brass nozzles, and both color and black and white photography was carried out to obtain images of the flame profiles. The burning velocities were calculated by dividing the dust flow rate through the nozzle by the flame surface area obtained through the flame profiles. From these studies the following conclusions can be made.

1) It is likely that the assumption of dust flames being an order of magnitude greater in flame thickness than gas flames may not be realistic. This can be seen by observing the relatively small tip curvature that a stable aluminum dust flame exhibits. An order of magnitude greater in flame thickness from a gas flame would have to imply a flame thickness of 10 mm or more in a dust flame. This would clearly yield a significantly wider tip curvature for any given condition (i.e. flow rate or nozzle diameter) than has been presently observed. Another condition that must be considered in flame thickness is the thermal gradient provided by the combustion zone. In a dust flame, this gradient would have to yield much lower burning velocities than the ones observed in order to overcome a 10 mm flame thickness. All this suggests that the actual dust flame thickness is most likely less than an order of magnitude

thicker than a gas flame. In addition, the present estimates have shown that the thickness of an aluminum dust flame is actually comparable to the thickness of the methane-air flame. In general, the relatively small thickness of the aluminum dust flame may also help explain why the profiles of the flame cones, seen by the aluminum oxide and sodium radiation filters, appeared to be very similar in both shape and size.

2) The flame curvature effect that may be responsible for the higher tip flame speeds in gas flames may also be responsible for the lower burning velocities observed in larger nozzles (and higher burning velocities in higher flow rates) in the present experiments. The apparent flame thickness did not vary much, whereas a wider tip curvature in large nozzle flames (compared to a smaller nozzle flames) was easily noticeable. Although the flame thickness in aluminum dust flames may not be an order in magnitude greater than gas flames, the dust flames are nonetheless much thicker than gas flames. In applying the Markstein curvature correction equation, it can be easily seen how the increase in flame thickness of aluminum dust flames will significantly affect the burning velocity of dust flames. The lack of noticeable change in dust flame shape (radius of curvature and surface area) when varying the experimental parameters (i.e. flow rate, nozzle diameter and concentration) may also help explain why the unperturbed burning velocity did no vary much throughout the experimental investigation, yielding a constant value irrespective of the varied parameters. From the present experimental results, it

can be seen how flame curvature may influence laminar burning velocities in stable aluminum dust flames significantly more than gas flames.

3) It is important to consider other important effects when studying gas-particle flows such as particle spacing and boundary layers which this present work has not been able to address in detail. An increase in particle concentration can significantly alter the state of a heterogeneous mixture by placing particles closer to one another, influencing the combustion process of individual particles and subsequently affecting the combustion of the dust mixture as a whole. Boundary layers are also affected in gas particle flows due to particle drag and may, in turn, influence the heat transfer processes that occur at the nozzle rim. Boundary layer effects may directly influence such conditions as flashback, blow-off and flame lifting.

4) The laminar burning velocity results obtained in this work prove the existence of a fundamental burning velocity for aluminum dust flames. The present experimental investigation has helped validate the dust burner as a valuable tool in obtaining fundamental dust flame parameters provided that the dust flame curvature effect as well as the stretch effect (when present) are taken into consideration.

5.2 Recommendations for Future Work

The present experimental investigation has successfully achieved its proposed objectives within the scope of the work: obtaining reliable data on the fundamental burning velocity of aluminum dust flames for the given particle size. However, much work is now needed to be carried out in order to further understand dust flames and their characteristic behavior. The following recommendations are proposed by the author in view of the recent findings of the present investigation.

1) The use of more advanced diagnostics and spectroscopy can be made to further analyze the light spectrum of the stable dust flame. This may give a more detailed structure of the stable dust flame by providing a more accurate distribution of species. More accurate data may be obtained pertaining to the reaction mechanisms and steps that occur within the dust combustion zone as well as the dust flame product zone.

2) In the present work the fuel used was aluminum powder of a 5 micron average particle size and a 99.5% purity content of aluminum. Since most modern applications of powders and dusts do not have such purity content, moreover the particle distribution (with the exception of lycopodium) in most commercially available powders is significantly wide, it would be of interest to carry out experiments on different particle sizes and different metallic fuels.

3) The use of digital photographic equipment may also be employed to produce more accurate flame images and directly analyzing them on computers rather than transferring images to a film scanner. A wider variation of optical filters may be used and better resolution may be obtained with digital imaging equipment.

4) Since the present work studied the laminar burning velocity of pre-mixed aluminum-air Bunsen flames, it would be of interest to pursue combustion research on other flame structures such as diffusion flames, flat pre-mixed flames and turbulent dust flames.

5) The complexities of two-phase flow were very briefly discussed in the present work, however, their implications on dust combustion phenomena can be significant and further investigation on the fluid dynamics as well as the thermodynamics of dust flows should be addressed in future research involving dust flames.

References

1. Smoot, L.D., Horton, M.D., "Propagation of Pulverized Coal-Air Flames", Proc. Energy Combustion Science., vol. 3, pp 235-258, 1977

2. Abrahamsen, A.R., "The U.K. Approach to Dust Explosibility Assessment and Its Relevance to Explosion Prevention and Protection", Industrial Dust Explosions, pp. 60-73, 1986

3. Grose, V.L., (edited by) "Explosion of DeBruce Grain Elevator Wichita, Kansas", U.S. Department of Labor, Occupational Safety and Health Administration. 1998

4. Energy Information Administration, "U.S. Energy Consumption by Source", U.S. Department of Energy Annual Review, 2001

5. Goroshin. S. V., Higgins. A.J., Lee. J.H.S., "Powdered Magnesium-Carbon Dioxide Propulsion Concepts For Mars Missions", 35th AIAA/ASME/SAE/ASEE Joint Propulsion Conference and Exhibit, 1999

6. Eckhoff, R.K., *Dust Explosions in the Process Industry*, Butterworth-Heinemann Ltd., Oxford, England, 1991

7. Pokhil, P., Belyaev, A., Frolov, Yu., Logachev, and A., Korotkov, A., Combustion of Powdered Metals in Active Media, NTIS, US Department of Commerce, 1973 (Translation)

8. Glassman, I., Sawyer, R.F., "The Performance of Chemical Propellants", AGARDograph, 129, Technivision Service, Slough, England. 1970

9. Branstetter, J.R., Lord, A. M., Gerstein, M., *Combustion Properties of Aluminum as Ramjet Fuel*, NACA Research Memorandum Lewis Flight Propulsion Laboratory, Cleveland, U.S., 1951

10. Bain, A., "The Hindenburg Disaster, A Compelling Theory of Probable Cause and Effect", PhD dissertation Dr. Addison Bain, 1998

11. Nusselt, W. "The Combustion Process of Pulverized Coal Firing", V.D.I., pp 124, 914, 1924

12. Ballal, D.R., "Flame Propagation Through Dust Clouds of Carbon, Coal, Aluminum and Magnesium in an Environment of Zero Gravity", Proc. R. Soc. London, A385, 21-51, Great Britain, 1983

13. Goroshin, S.V., Bidabadi, M., Lee, J.H.S., "Quenching Distance of Laminar Flames in Aluminum Dust Clouds", Comb. Flame 105: 147-160, 1996

14. Cassel, H.M., *Some Fundamental Aspects of Dust Flames*, Report of Investigation no.6551, U.S. Bureau of Mines, 1964

15. Cassel, H.M., Das Gupta, A.K., Guruswamy, S., "Factors Affecting Flame Propagation Through Dust Clouds", Proc. Comb. Inst. 3: 185-190, 1949

16. Goroshin, S.V., Fomenko, I., Lee, J.H.S., "Burning Velocities in Fuel-Rich Aluminum Clouds", Proc. Comb. Inst. 26: 1961-1967, 1996

17. Reist, P., *Aerosol Science and Technology*, McGraw-Hill, New York, U.S., 1993

18. Lewis, B., Von Elbe, G., *Combustion and Explosion of Gases*, Academic Press, New York, U.S. , 1987

19. Goroshin, S.V., Shoshin, Y.L., Ageyev, N.I., Poletayev, N.I., "The Premixed Aluminum Dust Laminar Flame Structure", Flame Structure, Vol. 2, Novosibirsk Nauka, Siberian Branch, USSR, 1991

20. Andrews, G.E., Bradley, D., "Determination of Burning Velocities: A Critical Review", Comb. Flame 18:133-153, 1972

21. Landau, L., "Theory of Slow Combustion", Acta Physicochim. 19, 77, USSR, 1944

22. Darrieus, G., "Propagation D'Un Front de Flamme. Essai de Théorie des Vitesse Anomales de Déflagration par Développement Spontané de la Turbulence", ^th International Congress of Applied Mechanics, Paris, France, 1946

23. Markstein, G.H., "Experimental and Theoretical Studies of Flame Front Stability", J. Aero. Sci. 18, 199, 1951

24. Markstein, G.H., (edited by) *Non-Steady Flame Propagation*, The Pergamon Press, New York, U.S., 1964